Bioactive Materials 9 (2022) 77–91

Contents lists available at ScienceDirect

Bioactive Materials

journal homepage: www.sciencedirect.com/journal/bioactive-materials

Effectiveness of an ocular adhesive polyhedral oligomeric silsesquioxane hybrid thermo-responsive FK506 hydrogel in a murine model of dry eye

Yi Han [a,1], Lu Jiang [b,1], Huihui Shi [c,d,1], Chenfang Xu [e,1], Minting Liu [e], Qingjian Li [a], Lan Zheng [a], Hong Chi [g], Mingyue Wang [g], Zuguo Liu [a], Mingliang You [f], Xian Jun Loh [d], Yun-Long Wu [e,**], Zibiao Li [b,h,***], Cheng Li [a,*]

[a] Fujian Provincial Key Laboratory of Ophthalmology and Visual Science & Ocular Surface and Corneal Diseases, Eye Institute & Affiliated Xiamen Eye Center, School of Medicine, Xiamen University, Xiamen, 361102, China
[b] Institute of Materials Research and Engineering, A*STAR (Agency for Science, Technology and Research), Singapore, 138634, Singapore
[c] School of Chemical Sciences, University of Chinese Academy of Science, Beijing, 100049, China
[d] Key Laboratory of Marine Materials and Related Technologies, Zhejiang Key Laboratory of Marine Materials and Protective Technologies, Ningbo Institute of Material Technology and Engineering, Chinese Academy of Science, Ningbo, 315201, China
[e] Fujian Provincial Key Laboratory of Innovative Drug Target Research and State Key Laboratory of Cellular Stress Biology, School of Pharmaceutical Sciences, Xiamen University, Xiamen, 361102, China
[f] Hangzhou Cancer Institute, Key Laboratory of Clinical Cancer Pharmacology and Toxicology Research of Zhejiang Province, Affiliated Hangzhou Cancer Hospital, Zhejiang University School of Medicine, Hangzhou, 310002, China
[g] Shandong Provincial Key Laboratory of Molecular Engineering, School of Chemistry and Pharmaceutical Engineering, Qilu University of Technology (Shandong Academy of Sciences), Jinan, 250353, China
[h] Department of Materials Science and Engineering, National University of Singapore, Singapore, 117575, Singapore

ARTICLE INFO

Keywords:
Ocular adhesive
Polyhedral oligomeric silsesquioxane
FK506
Dry eye

ABSTRACT

Dry eye is a common ocular disease that results in discomfort and impaired vision, impacting an individual's quality of life. A great number of drugs administered in eye drops to treat dry eye are poorly soluble in water and are rapidly eliminated from the ocular surface, which limits their therapeutic effects. Therefore, it is imperative to design a novel drug delivery system that not only improves the water solubility of the drug but also prolongs its retention time on the ocular surface. Herein, we develop a copolymer from mono-functional POSS, PEG, and PPG (MPOSS-PEG-PPG, MPEP) that exhibits temperature-sensitive sol-gel transition behavior. This thermo-responsive hydrogel improves the water solubility of FK506 and simultaneously provides a mucoadhesive, long-acting ocular delivery system. In addition, the FK506-loaded POSS hydrogel possesses good biocompatibility and significantly improves adhesion to the ocular surface. In comparison with other FK506 formulations and the PEG-PPG-FK506 (F127-FK506) hydrogel, this novel MPOSS-PEG-PPG-FK506 (MPEP-FK506) hydrogel is a more effective treatment of dry eye in the murine dry eye model. Therefore, delivery of FK506 in this POSS hydrogel has the potential to prolong drug retention time on the ocular surface, which will improve its therapeutic efficacy in the management of dry eye.

1. Introduction

Dry eye is a multifactorial ocular surface disease accompanied by tear film instability and hyperosmolarity. The inflammation caused by dry eye results in damage to the corneal epithelium and neurosensory abnormalities [1]. According to a clinical epidemiological investigation

Peer review under responsibility of KeAi Communications Co., Ltd.
* Corresponding author. Eye Institute of Xiamen University, 4th Floor, Chengyi Building, No. 4221-122, South Xiang'an Road, Xiamen, Fujian, 361102, China.
** Corresponding author. Fujian Provincial Key Laboratory of Innovative Drug Target Research and State Key Laboratory of Cellular Stress Biology, School of Pharmaceutical Sciences, Xiamen University, Xiamen, 361102, China.
*** Corresponding author. Institute of Materials Research and Engineering, A*STAR (Agency for Science, Technology and Research), Singapore, 138634, Singapore.
E-mail addresses: wuyl@xmu.edu.cn (Y.-L. Wu), lizb@imre.a-star.edu.sg (Z. Li), cheng-li@xmu.edu.cn (C. Li).
[1] Y. Han, L. Jiang, H. Shi and C. Xu contributed equally to this work.

https://doi.org/10.1016/j.bioactmat.2021.07.027
Received 8 March 2021; Received in revised form 21 July 2021; Accepted 21 July 2021
Available online 28 July 2021

by several research centers worldwide, the prevalence of dry eye ranges from 4.1% to 23.7% of the general population [2]. Prolonged use of digital devices such as smartphones, tablets, computers, etc. can be a factor damaging the ocular surface. As such exposure is on the increase, dry eye incidence is becoming more common, which reduces the quality of life and imposes a financial burden [3]. Eye drops containing FK506 (also named Tacrolimus), a hydrophobic macrolide immunosuppressant, are currently used to alleviate dry eye by blocking T cell-dependent immune reactions. However, FK506 is a highly hydrophobic substance with poor aqueous solubility in a range of 0.67 ± 0.19 μg/mL [4]. Its poor aqueous solubility might affect the drug efficacy, cause undesired ocular movement (such as blinking, tear turnover, and nasolacrimal drainage), reduce the ocular residence time of FK506 on the ocular surface, and lead to low bioavailability of commercial eye drops [5,6]. Adequate drug delivery typically requires increasing the drug administration frequency to four or five times daily to improve remediation of the condition; however, this elevates the risk of side effects. Therefore, it is necessary to design a drug delivery system that not only improves the water solubility of hydrophobic drugs but also prolongs their retention time on the ocular surface.

In recent years, various drug delivery systems, such as polymer micelles and hydrogel-based formulations, have been developed to improve drug solubility and retention time [7,8]. Hydrogel-based drug delivery systems are among these attracting much attention, thermo-responsive polymers are particularly noteworthy due to their intriguing ability to undergo sol-gel transformation [9]. Eye drops consisting of thermo-responsive polymers can be gelled *in situ* on the ocular surface, which makes them convenient to use [10]. In addition, after a hydrogel has formed, it improves the drug retention time on the ocular surface [11]; therefore, thermo-responsive polymers have great potential applications in eye-drop preparations [12].

Polyhedral oligomeric silsesquioxane (POSS), considered to be the smallest particle of silica (1–3 nm in diameter), has attracted increasing attention in the development of hybrid materials over the past few decades [13,14]. Formulated as $(RSiO_{1.5})_n$ (n = 6, 8, 10, 12, etc.), POSS has a characteristic inorganic Si–O–Si cage structure with hydrogen atoms or various organic groups on their vertex [15–17]. Due to its well-defined nanostructure and precise chemical modification, POSS derivatives can be physically or chemically incorporated into polymer matrices with high compatibility, resulting in strengthened mechanical properties, enhanced thermal stability, excellent optoelectronic performance, and superhydrophobicity, which are promising properties for a wide range of applications [18–21].

Hydrogels are another well-studied candidate for biomaterials and comprise hydrophilic polymeric networks capable of absorbing a large amount of water [22]. Their elastic and soft nature offers similarity and biocompatibility with living tissues, and their network structure provides permeability for small molecules [23]; thus, hydrogels have been widely used in drug delivery, tissue engineering, wound dressing, and contact lenses [24–26].

Recently, some researchers have become interested in combining POSS and hydrogels to fabricate nanocomposite hydrogels [27]. Andrzejewska et al. used octa-methacrylate POSS as a chemical crosslinker and copolymerized it with mono- and di-methacrylated poly(ethylene glycol) (PEG), conceiving hydrogels with enhanced Young's modulus, tensile strength, and hardness [28]. Xu et al. reported temperature and pH dual-responsive hydrogels based on poly(N-isopropylacrylamide) (PNIPAM) and poly(dimethylaminoethyl methacrylate) co-crosslinked by octa-vinyl POSS and N,N′-methylenebisacrylamide (MBA), which exhibited improved compressive strength and a faster swelling/deswelling rate [29]. Zhang et al. added octa-amino POSS into a PNIPAM system as an imitator and a physical crosslinker in the presence of a small amount of MBA, chemical crosslinker, which produced hydrogels that exhibit self-healing ability [30]. With respect to mono-functional POSS, Yang et al. used POSS as an end-cap for blocking copolymers of PEG and bisuream. Physical hydrogels were obtained with crosslinking points formed from the aggregation of POSS as well as hydrogen bonding of bisream. This modification had enhanced mechanical properties and shear-thinning behaviors [31]. Mather et al. copolymerized PEG and diol POSS with a urethane linkage. Furthermore, the copolymers could be easily processed into thin films at a high temperature and swollen to stiff hydrogels with tunable physical properties dependent on the POSS content [32]. Several studies have demonstrated that the addition of POSS components to hydrogels contributes to cell adhesion and proliferation on scaffolds [33], which played an important role in enhancing the adhesion between the hydrogel and the ocular surface. Together with the low toxicity, good biocompatibility, and specific bioactivity, hydrogels containing POSS have been regarded as a promising drug delivery system for the ocular surface.

In the present work, we synthesized a series of polyurethane-based copolymers from macrodiols of MPOSS, PEG, and PPG blocks, which were endowed with temperature-sensitive sol-gel transition behaviors. Due to the strong hydrophobicity of POSS, we assumed that its introduction would promote the self-assembly of copolymers and have an impact on micellization and gelation properties, further increasing its application in biomedicine. The thermo-responsive hydrogel containing POSS improved the water solubility of FK506 and increased adhesion between the ocular surface and the hydrogel, prolonging the drug retention time and leading to improved resolution of dry eye. The present study focused on the molecular characteristics, self-assembly properties, sol-gel transition behaviors of the copolymers, and explored their potential for treatment of dry eye. Moreover, the results indicate that this hydrogel possesses good biocompatibility and significantly improves adhesion to the corneal surface. Furthermore, in comparison with Commercial FK506 and PEG-PPG-FK506 (F127-FK506) hydrogel, the MPOSS-PEG-PPG-FK506 (MPEP-FK506) hydrogel has a greater therapeutic efficacy in dry eye.

2. Experimental section

2.1. Synthesis of poly(MPOSS-PEG-PPG urethane) (MPEP) copolymers

Poly(MPOSS-PEG-PPG urethane) (MPEP) was derived from macrodiols of MPOSS, PEG, and PPG, with the feed ratio of PEG-PPG (F127) fixed at 2:1, HDI as the chain extender, and DBT as the catalyst. The synthetic method was similar to that used in our previous work [34]. The MPOSS content was set at 0.5, 1, or 2 wt%, and the resulting copolymers were denoted as *n*MPEP, where *n* represented the feed weight percentage of MPOSS: MP for MPOSS, E for PEG, and P for PPG. Additional details are provided in the Supporting Information.

2.2. Molecular characterization

Gel permeation chromatography (GPC) was conducted on a Waters GPC System (Shimadzu, Japan) equipped with two Phenogel columns (103 and 105 Å) (size: 300 × 7.80 mm) in series and a refractive index detector. HPLC grade THF was used as an eluent at a flow rate of 1 mL/min at 40 °C. Poly(methyl methacrylate) standards were used to generate a calibration curve.

^{1}H and ^{13}C nuclear magnetic resonance (NMR) spectra were obtained using a 500-MHz NMR spectrometer (JEOL, Japan) at room temperature. The chemical shift was referenced to the solvent peak of $CDCl_3$ at 7.3 ppm.

Fourier transform infrared (FT-IR) spectra were collected using a Spectrum 2000 FT-IR spectrophotometer (PerkinElmer, USA) at room temperature. The copolymers were mixed with KBr and tableted, undergoing 32 scans in the wavenumber range of 4000–400 cm^{-1} at a resolution of 4 cm^{-1}.

2.3. Thermal analysis

Thermogravimetric analysis (TGA) was carried out on a Q500 TGA

analyzer (TA Instruments, USA) under a nitrogen atmosphere. The temperature was elevated from room temperature to 800 °C at a rate of 20 °C/min.

Differential scanning calorimetry (DSC) was performed on a Q100 photo-DSC analyzer (TA Instruments, USA) using indium for calibration. Two heating−cooling cycles in the range of −80 °C to 200 °C were run at a heating or cooling rate of 20 °C/min, and data from the second cycle were used for analysis.

2.4. Determination of the critical micelle concentration (CMC)

Aqueous copolymer solutions at different concentrations starting from 1 wt% were prepared using the gradient dilution method, and then mixed with DPH methanol solution (0.6 mM) at a volume ratio of 50:1. After reaching equilibrium at 4 °C overnight, UV–vis spectra were obtained on a UV-2501 PC spectrophotometer (Shimadzu, Japan) at room temperature in the range of 320–460 nm.

2.5. Particle size analysis

The particle size and distribution of the aqueous copolymer solutions at different concentrations (0.1, 0.5, and 1 wt%) and different temperatures (25, 37 and 70 °C) were measured by dynamic light scattering (DLS) on a Nano ZetaSizer System (Malvern Instruments, USA) using a 633-nm laser light and a scattering angle of 173°.

2.6. Determination of the lower critical solution temperature (LCST)

The LCST value of the aqueous copolymer solutions (2 wt%) was also estimated by UV–vis spectra generated on a UV-2501 PC spectrophotometer (Shimadzu, Japan) equipped with a temperature control module. The temperature was elevated from 25 °C to 75 °C at an interval of 1 °C and an equilibrium time of 5 min per step.

2.7. Determination of sol-gel transition behaviors

Aqueous copolymer solutions at concentrations varying from 2 wt% to 20 wt% were prepared in 4-mL vials. After being placed at 4 °C for 1 d to ensure full dissolution, the samples were gradually heated in a water bath from 4 °C to 80 °C at an increment of 2 °C and an equilibrium time of 5 min per step. The gelation temperature was defined as the critical temperature at which firm gels were observed in inverted vials.

2.8. Rheological analysis

The rheological measurements were performed on a Discovery DHR-3 hybrid rheometer (TA Instruments, USA) adopting a parallel-plate geometry. Temperature ramps from a low temperature to body temperature and temperature sweeps from 4 °C to 80 °C at a heating rate of 5 °C/min were measured, both with the strain fixed at 1% and the frequency fixed at 1 Hz.

2.9. Determination of the light transmittance of blank hydrogel

Temperature-sensitive copolymers, 1MPEP and 2MPEP, can form hydrogels at ocular surface temperature (34.5 °C) at a concentration of 5%, while the concentration of F127 needs to reach 20% [35]. PBS solutions containing 5% 1MPEP, 5% 2MPEP, and 20% F127 were prepared. A 100-μL aliquot of the samples was placed in a 96-well plate and incubated 34.5 °C to form hydrogels; a commercial liquid Carbomer was used as a control. A multifunctional microplate reader (Multiskan FC, Thermo Fisher Scientific, USA) was used for full-wavelength scanning to determine the absorbance value. The light transmittance of the hydrogel was calculated according to the formula, A = –log T%, where A is absorbance and T% is light transmittance [36]. According to previous studies, hydrogels with a light transmittance greater than 90% in the visible wavelength range of 390–780 nm are considered transparent; those with a light transmittance of 10–90% are considered translucent; and those with a light transmittance below 10% are considered opaque [37].

2.10. Degradation analysis of blank hydrogel

A 500-μL aliquot of 1MPEP, 2MPEP, and F127 solution was added to a microfuge tube. After the hydrogel had formed at 34.5 °C, 500 μL PBS was gently added on top of the hydrogel. The microfuge tubes were placed vertically in a constant-temperature shaker, and degradation was carried out at 34.5 °C and 50 rpm. At a specific timepoints, the upper liquid was removed and the tubes were weighed; the weight of the remaining hydrogel was recorded following subtraction of the weight of the blank tube, and fresh PBS was subsequently added to continue degradation.

2.11. Determination of the concentration of FK506 by high-performance liquid chromatography (HPLC)

HPLC was used to determine the concentration of FK506. Column: ZORBAX SB-C18 (5 μm, 4.6 × 150 mm); mobile phase: acetonitrile: 0.25% phosphoric acid aqueous solution (60:40, v/v); UV detection wavelength: 215 nm; flow rate: 1 mL min^{-1}; column temperature: 50 °C; injection volume: 10 μL.

FK506 powder was accurately weighed and dissolved in acetonitrile at a concentration of 1 mg/mL for use as a stock solution. FK506 was serially diluted in the mobile phase to generate standards of 1, 2, 4, 12, 24, 32, 64, and 128 μg/mL. Each solution was subjected to chromatography, and a concentration–peak area standard curve was created. The fitted curve was $y = 19.059x + 13.581$, $R^2 = 0.9999$.

2.12. Preparation of the FK506 hydrogel

Since FK506 is poorly water-soluble, it was first wrapped in amphiphilic micelles. At a material/drug ratio of 20:1, 1MPEP, 2MPEP, F127, and the same amount of FK506 was dissolved in acetone and the mixture was added dropwise to PBS while stirring. Nitrogen blowing was used to remove the volatile acetone to prepare 1MPEP-FK506(1M-FK506), 2MPEP-FK506(2M-FK506), and F127-FK506 drug-loaded micelle solutions. The precipitate was removed by centrifugation at 2000 rpm, and HPLC determined the FK506 concentration in the supernatant. Its concentration was then calculated and adjusted. A certain weight of material was added to ensure that the final concentration of 1MPEP, 2MPEP, and F127 was approximately 5%, 5%, and 20%, respectively. The final concentration of FK506 was set to 0.1% according to the commonly used clinical concentration and stored for use.

2.13. In vitro drug release experiment

A 500-μL aliquot of 1M-FK506, 2M-FK506, or F127-FK506 solution was added to a microfuge tube and allowed to form hydrogels at 34.5 °C in a constant-temperature water bath. Subsequently, 500 μL 1 × PBS (containing 0.2% Tween) was gently added to the top of the hydrogel as the release medium. The tubes were placed vertically in a constant-temperature shaker at 50 rpm and 34.5 °C. The upper release medium was removed at certain timepoints and replaced with 500 μL fresh PBS until the hydrogel had completely degraded. The release medium was subjected to HPLC to measure the concentration of FK506, which was used to construct a drug release curve.

2.14. Cytotoxicity of the hydrogel on human corneal epithelial (HCE) cells

The drug solutions were prepared using the same method as that for the hydrogel extract. The 1MPEP, 2MPEP, F127, 1M-FK506, 2M-FK506,

and F127-FK506 solutions were stored at −80 °C for three days, following which 500 μL of each was added to a cell culture plate and allowed to form a hydrogel at 37 °C. Subsequently, 1 mL of the culture medium was added and incubated at 37 °C for 48 h. The supernatant was collected and serially diluted with medium to obtain 0.5, 0.25, 0.125, 0.0625, and 0.03125 mg/mL; the 0 mg/mL FK506 group was used as a control.

The MTT assay was used to assess cell viability. The immortalized human corneal epithelial (HCE) cell line was purchased from the American Type Culture Collection (ATCC) and cultured in DMEM/F12 medium supplemented with hEGF, insulin, FBS, and penicillin-streptomycin. HCE cells were seeded onto 96-well plates and incubated for 24 h. The diluted hydrogel–drug extracts were added and incubated for 48 h, following which the medium was removed, replaced with MTT solution, and incubated for another 4 h. The supernatant was removed and replaced with DMSO to dissolve the formazan crystals. Finally, the absorbance was measured at 492 nm using a SpectraMax® absorbance reader (Molecular Devices); cell survival curves were subsequently constructed.

2.15. Surface plasmon resonance

Surface plasmon resonance on a BIAcore-T200 biomolecular interaction analyzer was used to analyze the interaction between mucin and polymers. The purchased mucin was dialyzed in ice-cold PBS for 48 h to replace the salt content in the original sample, and the protein was subsequently freeze-dried. Acetate buffers of different pH were configured to screen the appropriate pH for protein coupling. The amino coupling method was used to fix mucin on the CM5 sensor chip, with the final immobilization level of mucin being approximately 10,000 RU. Using PBS as the working buffer, 1MPEP, 2MPEP and F127 were serially diluted to 62.5 μM, 31.25 μM, 15.625 μM, 7.8125 μM, 3.90625 μM, and 0 μM. The polymer solution at various concentrations was passed over the chip with a contact time of 120s, a flow rate of 30 μL/min, and a separation time of 450s. The chip was subsequently washed with pH 2.5 glycine buffer and PBS buffer at a working temperature of 25 °C. Biacore T200 Evaluation software (Version 2.0) was used to analyze the interaction between mucin and polymers, and the curve was fitted with a 1:1 binding model to calculate the kinetic constant KD value.

2.16. Animal dry eye model

Female C57BL/6 mice (weighing 25–35 g; aged 8–12 weeks) were purchased from the Animal Center of Xiamen University (Xiamen, Fujian, China). The animal protocols conformed to the Association for Research in Vision and Ophthalmology (ARVO) Statement for the Use of Animals in Ophthalmic and Vision Research. This research program was approved by the Experimental Animal Ethics Committee of Xiamen University. The mice were kept in a well-ventilated environment at a humidity of 30 ± 3% and a temperature of 23–25 °C. Subcutaneous injections of scopolamine hydrobromide (0.25 g/100 mL) in the flank four times daily for five days established a desiccating stress (DS5) [38–40].

2.17. Topical drug treatment and slit-lamp imaging

Topical drug treatment was performed on the murine dry eye model by applying 5 μL different eye drops formulation (PBS, 1MPEP, 2MPEP, F127, Commercial FK506, F127-FK506, 1M-FK506, 2M-FK506) twice daily for five days without anesthesia. In detail, researchers gently held a mouse and tried their best to comfort it before performing subcutaneous injection with minimal pain and stress. Besides, all the researchers received training, into how to skillfully administer the subcutaneous injection to avoid secondary injury to the mouse.

Following administration of the eye drops and manual blinking of the murine eyes, the corneas were examined and imaged via slit-lamp microscopy to observe the hydrogel on the ocular surface. The process was performed as described previously [41].

2.18. Tear secretion test

The tear secretion test was performed at the end of treatment. Briefly, a phenol red cotton thread was placed into the lower conjunctival fornix and the mouse was forced be stay stationery for 15 s. The secretory rate was measured in millimeters based on the advancement of the red stained tear front.

2.19. Corneal fluorescein staining

Corneal fluorescein staining was conducted by instilling 5% Oregon green dextran (OGD) onto the murine ocular surface for 1 min with manual blinking several times. The mice were subsequently euthanized, and the corneas were rinsed with 1 mL saline five times. The corneas were photographed using a fluorescence dissecting microscope (Leica, Wetzlar, Germany) under 470-nm fluorescence excitation. The fluorescence intensity of corneal OGD staining was quantitatively analyzed using the NIS Elements software (NIS Elements; version 4.1; Nikon, Melville, NY, USA) with a 200,000-pixel circle on the central cornea.

2.20. Histological staining

The murine eyeballs and periocular adnexa were separated and harvested, fixed in 4% formaldehyde for at least 24 h, and infiltrated with paraffin. Paraffinized samples were cut into sagittal sections (5-μm thick), placed on glass slides, and stained using Hematoxylin & Eosin (H&E) and Periodic Acid-Schiff (PAS) staining kits according to the manufacturer's instructions. All stained slides were observed and imaged using a light microscope (Eclipse E400 with a DS-Fi1, Nikon, Melville, NY). For PAS staining, the goblet cells were quantitatively counted using the NIS Elements software including the upper and lower conjunctiva.

2.21. Immunofluorescence staining

After sampling, the tissues were embedded in optimal cutting temperature compound (OCT compound) and stored at −80 °C. Frozen samples were cut into sagittal sections (5-μm thick) and placed on glass slides. For immunofluorescence staining, following fixation in acetone and blocking with 2% bovine serum albumin (BSA), the frozen slices were incubated at 4 °C overnight with anti-matrix metalloproteinase-3 (MMP-3), anti-matrix metalloproteinase-9 (MMP-9), and anti-CD4 antibodies. The following day, the slices were washed in PBS three times and incubated with Alexa Fluor 488-conjugated donkey anti-goat IgG or Alexa Fluor 488-conjugated donkey anti-rabbit IgG for 1 h in the dark at room temperature. Lastly, the slices were mounted with DAPI, observed and then imaged using a fluorescence microscope (LeicaDM2500).

2.22. Western blotting

Murine conjunctival tissues were surgically separated and dissolved in cold RIPA buffer containing protease and phosphatase inhibitor cocktail. The protein solutions were extracted, purified, and subsequently quantitated using a BCA assay kit. Equal amounts of protein were separated on 12% tricine gels and transferred to polyvinylidene difluoride (PVDF) membranes. The membranes were blocked in 5% BSA for 2 h at room temperature, followed by overnight incubation with an anti-CD4 antibody. The next day, the membranes were washed three times with Tris-buffered saline containing 0.05% Tween 20 (TBST), and the membranes were incubated for 1 h with HRP-conjugated goat anti-rabbit IgG. Protein bands were visualized using an Ultra Chemiluminescence Reagent kit and images were captured by the ChemiDoc XRS System (BioRad Laboratories, Inc., Philadelphia, PA, USA).

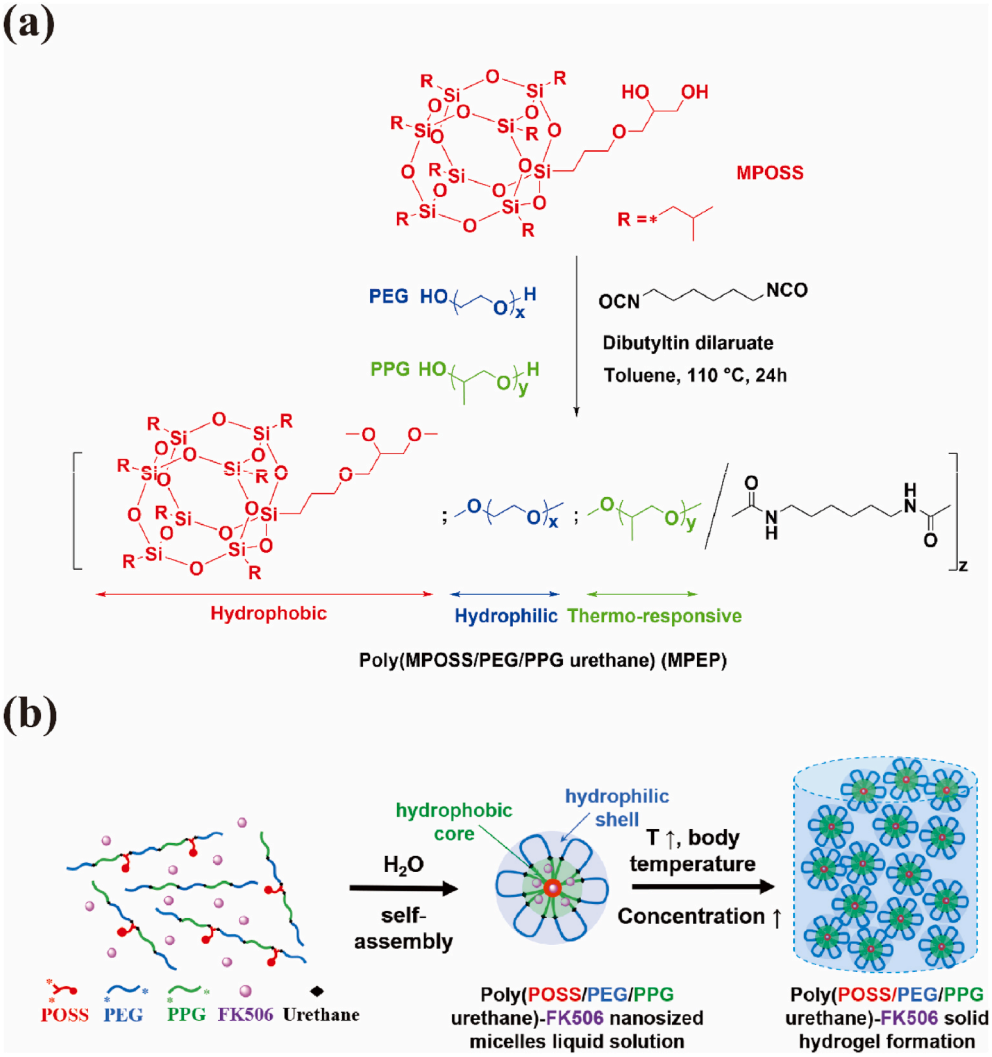

Scheme 1. (a) Synthesis of MPEP by polyaddition and (b) illustration of the self-assembly of MPEP and hydrogel formation in water.

Densitometry was performed using the ImageJ software.

2.23. Optical coherence tomography (OCT) examination, fundus imaging, and fluorescence fundus angiography

OCT, fundus imaging, and fluorescence fundus angiography were performed using an OPTOPROBE system (China). Briefly, different FK506-containing eye drops (Commercial FK506, F127-FK506, 1M-FK506, 2M-FK506) were administered twice daily for 7days, following which the mice were anesthetized by abdominal cavity injection of 1% pentobarbital sodium (0.0075 mL/g), and tropicamide phenylephrine eye drops were used to dilate the pupils. Retinal OCT and fundus images of each eye were captured, centered on the optic nerve head. Corneal OCT images were conducted in the same manner as the retinal OCT process following administration of the drugs and manual blinking. Prior to fluorescence fundus angiography, the mice were injected with 1% fluorescein sodium (0.0075 mL/g) in the abdominal cavity. Fluorescence fundus angiography images were captured in the same manner as the fundus imaging process.

Table 1
Molecular characteristics and properties of MPEP copolymers.

Sample	Feed ratio/g			Composition/wt%[a]			GPC results		Thermal properties				Char yield/%
	MPOSS	PEG	PPG	MPOSS	PEG	PPG	M_n	$Đ_M$	T_d/°C[b]	T_c/°C[c]	T_m/°C[d]	T_g/°C[e]	
0.5MPEP	0.05	6.63	3.32	0.4	71.7	28.5	29666	1.63	320.41	−18.07	38.21	−56.81	0.26
1MPEP	0.1	6.60	3.30	0.8	68.6	30.6	36761	1.74	299.03	−19.07	38.41	−56.05	2.50
2MPEP	0.2	6.53	3.27	1.8	67.4	30.8	34154	1.83	316.62	−19.34	37.15	−58.02	3.24
MPOSS	/	/	/	/	/	/	/	/	266.23	144.62	162.05	/	
PEG2000	/	/	/	/		/	/	/	/	33.15	55.13	/	

[a] Calculated from the ^{1}H NMR spectra.
[b] Degradation temperature determined by TGA.
[c] Crystallization temperature determined by DSC.
[d] Melting temperature determined by DSC.
[e] Glass transition temperature determined by DSC.

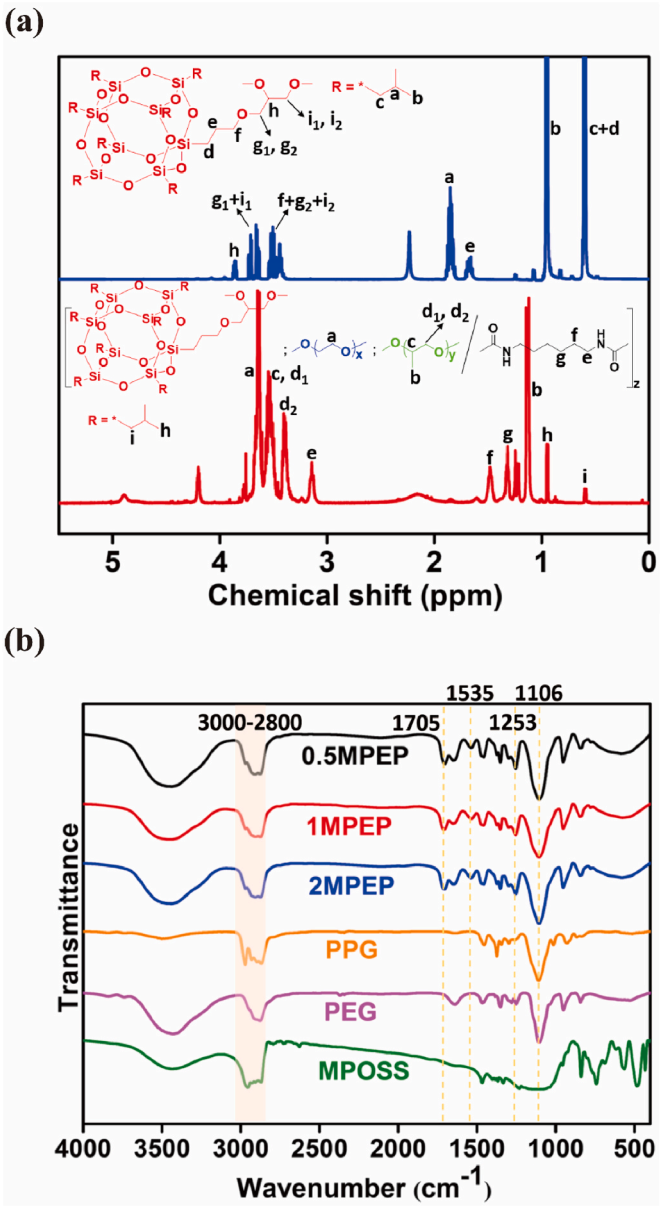

Fig. 1. (a) ^{1}H NMR spectra of MPOSS (blue line) and 2MPEP (red line) in $CDCl_3$. (b) FT-IR spectra of MPOSS, PEG, PPG, and three MPEP copolymers. (For interpretation of the references to colour in this figure legend, the reader is referred to the Web version of this article.)

2.24. Statistical analysis

All data are expressed as the mean ± standard error of mean (S.E.M.). Based on the normality of the data distribution, statistical significance was evaluated by one-way ANOVA followed by Tukey's *post-hoc* test using the GraphPad Prism 8.0 software (GraphPad Software; San Diego, CA, USA). $P < 0.05$ was considered statistically significant.

3. Results and discussion

3.1. Molecular characteristics of poly(MPOSS-PEG-PPG urethane) (MPEP) copolymers

Random multiblock copolymers, poly(MPOSS-PEG-PPG urethane) (MPEP), with various amounts of MPOSS were synthesized from the polyaddition of MPOSS, PEG, and PPG, which were linked by diisocyanate HDI under a DBT catalyst (Scheme 1a). According to the GPC results in Table 1 and Fig. S3, the MPEP copolymers share a similar molecular weight and dispersity ($Đ_M$). After a 24 h reaction, there were 15–18 blocks on average in each polymer chain.

The chemical structures of the MPEP copolymers were verified by both the ^{1}H NMR and ^{13}C NMR spectrum (Fig. 1a, S1 and S2). Typically, PEG blocks have characteristic peaks at 3.6 ppm generated by CH_2. PPG blocks present peaks at 1.1 ppm, 3.4 ppm, and 3.5 ppm belonging to CH_3, CH_2, and CH, respectively. HDI linkages show specific peaks at 1.3 ppm, 1.5 ppm, and 3.1 ppm ascribed to CH_2 groups [42]. Referring to the ^{1}H NMR spectrum of MPOSS, the presence of MPOSS blocks in MPEP copolymers was confirmed by peaks at 0.9 ppm and 0.6 ppm that were attributed to seven CH_3 and CH_2 on the isobutyl groups. The integral ratio of all of these peaks is consistent with the theoretical value. A detailed description of the ^{13}C NMR spectrum is provided in the Supporting Information. Moreover, the composition of the MPEP copolymers was calculated from the integral ratio and it was close to the feed ratio (Table 1).

The similarity between the FT-IR spectra of the MPEP copolymer and their macrodiols yielded further evidence that the synthesis protocol was successful (Fig. 1b). New absorption bands appeared at around 1705 cm^{-1} and 1535 cm^{-1}, representing C═O and N–H in the urethane linkage generated from the hydroxyl/isocyanate reaction [43]. An overlapping absorption band for C–O–C in PEG and PPG blocks, as well as Si–O–Si in the MPOSS block, was observed at around 1106 cm^{-1}. A small amount of MPOSS also produces a moderate absorption band at around 1253 cm^{-1} with Si–C [44]. In addition, absorption bands in the range of 3000–2800 cm^{-1} corresponded to saturated C–H existing in all three blocks.

The thermal properties of MPEP copolymers were studied by TGA and DSC, and the relative parameters are shown in Table 1. The TGA results demonstrate good thermal stability of all three copolymers, whose degradation temperature for 5% weight loss was above 300 °C. Meanwhile, MPOSS underwent two steps of degradation after 266 °C and after 392 °C, attributed to the decomposition of vertex groups and transformation of the Si–O–Si cage structure into ceramics, respectively (Fig. 2a) [45]. Such changes were reflected in the TGA curves of MPEP copolymers, where the first step overlaps with the degradation of PEG and PPG blocks and the second step takes place after roughly 570 °C.

Regarding the DSC results, a single T_g for MPEP copolymers is presented in the heating process (Fig. 2d), indicating good miscibility of MPOSS with polymers and no microphase separation. The heating curve of MPOSS exhibits two endothermic peaks at 0 °C and 162 °C, likely corresponding to two crystal types (Fig. 2c) [46]. When incorporated into the polymer system, bulk aggregation of MPOSS is restricted due to its low content. Thus, for MPEP copolymers, only one endothermic peak caused by PEG blocks was observed at around 38 °C, lower than the T_m of pure PEG as a consequence of copolymerization. In reverse, the cooling curves of MPEP copolymers show an exothermic peak at around −19 °C with a weak shoulder on the left (Fig. 2b), which may be due to the wide distribution of molecular weight [47].

3.2. Self-assembly properties of MPEP copolymers

In aqueous solution, amphiphilic MPEP copolymers tend to self-assemble from unimers into micelles, driven by hydrophobic interaction. With a hydrophobic core of MPOSS and PPG blocks and a hydrophilic corona of PEG blocks, such micelles can encapsulate hydrophobic molecules in aqueous solution, thus yielding stabilization and solubilization effects [48]. Based on this, CMC values for MPEP copolymers were determined according to the UV–vis absorption spectrum using hydrophobic DPH as the fluorescent probe. Increasing the concentration from 0.0005 to 1 wt% caused the absorption peaks at around 344, 358, and 378 nm to become increasingly larger (Fig. 3a). By plotting graphs of the difference in absorbance at 378 nm and 400 nm (A_{378}–A_{400}) versus logarithmic concentration, CMC values of 0.5MPEP, 1MPEP, and 2MPEP were estimated to be 0.082 wt%, 0.075 wt%, and 0.071 wt%,

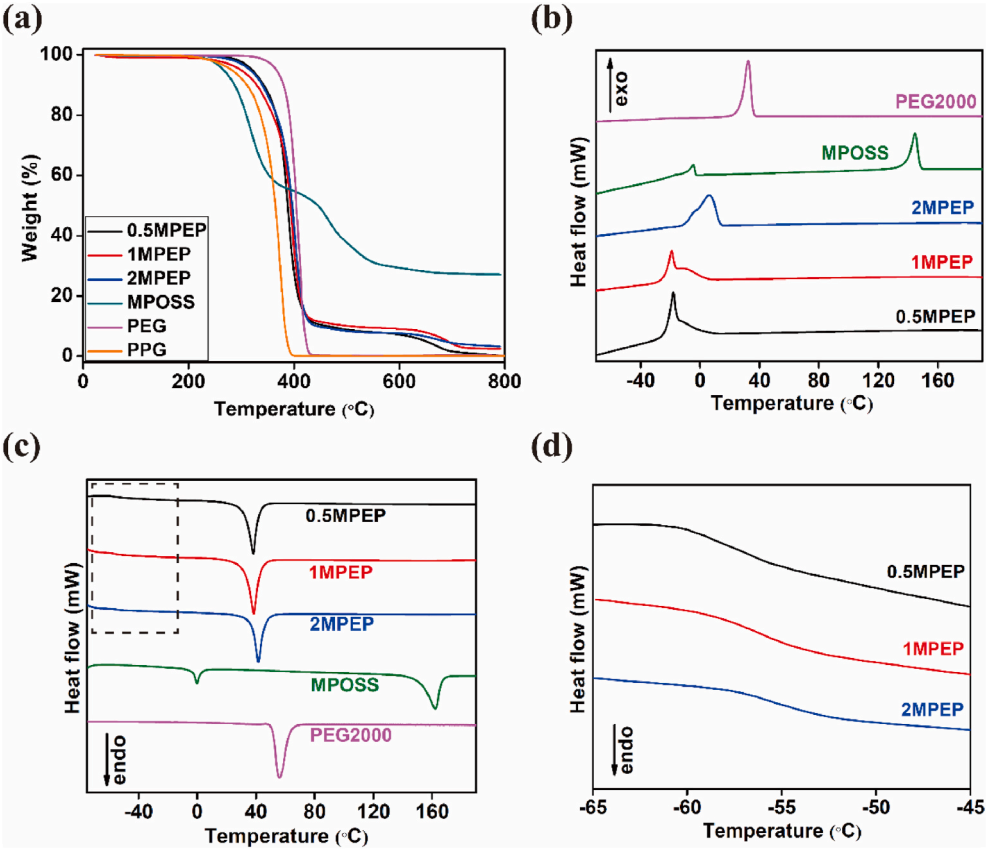

Fig. 2. (a) TGA curves of MPOSS, PEG, PPG and three MPEP copolymers. (b) DSC cooling curves of MPOSS, PEG, and MPEP copolymers. (c) DSC heating curves of MPOSS, PEG, and MPEP copolymers. (d) Enlarged graph of the dotted box in (c), indicates the glass transition temperature (Tg) range of MPEP copolymers.

respectively, decreasing slightly with increasing MPOSS content (Fig. 3b and S4).

Since PPG is inherent to a hydrophilicity/hydrophobicity transition depending on temperature, the self-assembly behaviors would change in order to reach the delicate balance between hydrophilicity and hydrophobicity. As illustrated in Scheme 1b, the micelles formed by MPEP were further reversibly aggregated at higher temperatures or concentrations. On the macro level, the aqueous MPEP solution turns cloudy, and the temperature at which a 50% reduction in the transmittance at 500 nm occurs is typically defined as the LCST for copolymers at that given concentration [49]. From Fig. 3c, it can be seen that the LCST values for MPEP copolymers adapted according to MPOSS content, which were estimated to be 53.6 °C for 0.5MPEP, 60.0 °C for 1MPEP, and 66.0 °C for 2MPEP at a concentration of 2 wt%.

The assumption of such micelle transformation at low concentrations was also confirmed by the change in particle size. The mean diameters of the particles in aqueous MPEP solution at different temperatures and concentrations as measured by DLS are shown in Table 2 (Supporting Information). By comparison, the samples mostly demonstrated a minor decrease in particle size when the temperature was increased from 25 °C to 37 °C. Different levels of particle size increase were observed after heating the samples to 70 °C, which is more evident at relatively higher concentrations due to the larger portion of micelle aggregates (Fig. 3d, 3e). Moreover, the MPOSS content of copolymers also affected the particle size, especially at relatively high temperatures. As shown in Fig. 3f, the particle size at 70 °C is positively correlated with MPOSS content, and the variation among different concentrations also increased because of the strong hydrophobicity of MPOSS which can facilitate the self-assembly and aggregation of micelles [50]. A detailed description of the MPEP copolymer morphology is provided in Supporting Information.

3.3. Sol-gel transition behavior of MPEP copolymers

Furthermore, as the concentration of aqueous MPEP solution continued to increase, the micelles they first packed into a network and then gradually became a non-flowable gel (Scheme 1b). Our group also reported that block copolymers from methacrylate POSS monomers and PEG macroinitiators self-assemble into micelles and as their concentration increases, they next become packed into macrogels. Moreover, more robust hydrogels were obtained by adding octa-vinyl POSS and carrying out UV curing [50,51]. The sol-gel transition behaviors of MPEP copolymers were investigated by the tube-inverting method. From the temperature- and concentration-dependent phase diagrams (Fig. 4a, S5a and S5b), aqueous MPEP solution may undergo four periods, including clear sol, clear gel, turbid gel, and dehydrated gel, as the temperature increases from 4 °C to 80 °C. Among these, the boundary between clear and turbid gels was hard to identify and they were classified together as being in the gel phase. In contrast, commercially available Pluronic F127 (PEG-PPG) underwent three transitions, including clear sol, clear gel, and clear sol (Fig. 4b). The opaqueness of MPEP thermogels probably results from the special mesh size of their micelle networks close to the visible-light wavelength. A different final state may be due to excessive hydrophobic interactions among multiple MPOSS and PPG blocks, which collapses micelle networks and repels water at high temperatures [52]. Moreover, it is obvious that the critical gelation temperature (CGT) for MPEP copolymers decreases with increasing concentrations and is controlled by MPOSS content. At the same concentration, a lower CGT is presented for MPEP copolymers with a higher MPOSS content. Meanwhile, the CGC for 0.5MPEP, 1MPEP, and 2MPEP was estimated to be 7 wt%, 5 wt%, and 5 wt%, respectively, which is much lower than that of Pluronic F127 and advantageous for biomedical applications.

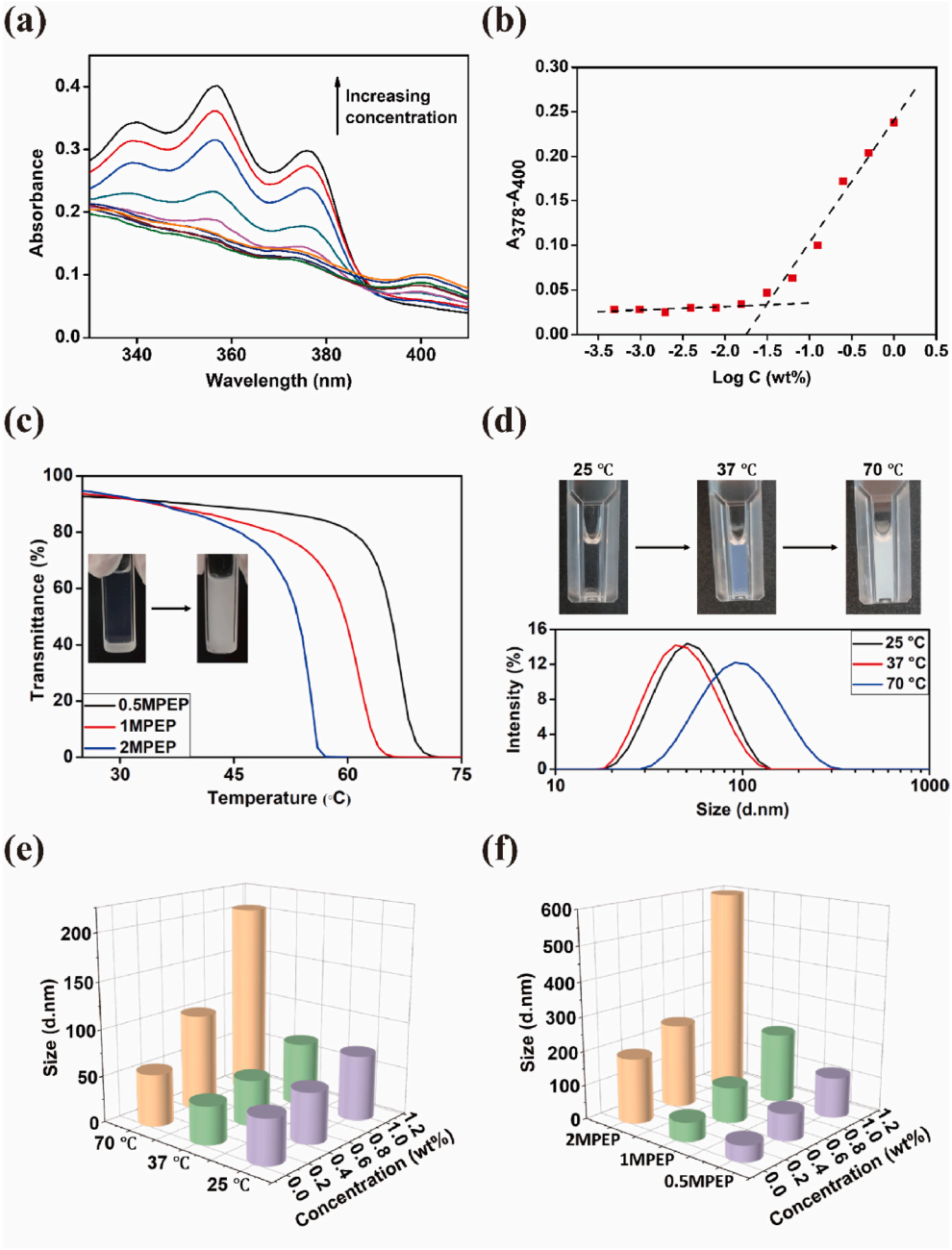

Fig. 3. (a) UV–vis spectra of aqueous DPH-1MPEP solution at a series of MPEP concentrations at room temperature. (b) CMC determination of 1MPEP by extrapolation. (c) Transmittance at 500 nm of aqueous MPEP solution (2 wt%) with increasing temperature. (d) Size distribution of micelles in aqueous 1MPEP solution (0.5 wt%) at three temperatures. (e) Particle size in relation to temperature and concentration in aqueous 1MPEP solution. (f) Particle size in relation to MPEP type and concentration in aqueous solution at 70 °C.

As a previous study indicated that POSS incorporation into the polymer chain markedly altered the rheological behavior of copolymers [53]. Rheological measurements were used to characterize the temperature responsiveness of MPEP copolymers. The concentrations of the tested samples were chosen to be 8 wt% for 0.5MPEP, 6 wt% for 1MPEP, and 5 wt% for 2MPEP, whose corresponding CGT values in the phase diagrams were approximately 32 °C, 24 °C, and 26 °C. According to the temperature sweep results over a the range from 4 to 80 °C (Fig. 4c, S5c, S5d), the storage modulus G′ and loss modulus G″ both increased with rising temperature at different rates and exhibited a crossover representing the sol-gel transition. The CGT determined from this method was approximately 32.0 °C, 16.3 °C, and 17.8 °C for 0.5MPEP, 1MPEP, and 2MPEP, respectively. While the CGT of 0.5MPEP obtained by the two methods matches well, the other two data points obtained from rheological measurements were lower than those obtained from the phase diagrams, probably because the temperature at which G′ is equal to G″ is actually a semi-solid state and not firm enough to be regarded as a gel in the tube-inverting method. From a temperature of approximately 70 °C, G′ and G″ began to decrease slightly and then became close again, which suggests the collapse of gels and coincides with the results of the tube-inverting method. In addition, the temperature ramp from a lower temperature such as 15 °C to body temperature was conducted to evaluate the response rate of the materials to the temperature change. As can be seen from Fig. 4d, S5e, and S5f, a fast sol-gel transition occurred that was almost in sync with the temperature change. This agreement is promising for utilizing injectable materials for *in situ* formation of hydrogels in biomedical applications. The temperature of the healthy corneal surface is around 34.5 °C, administering the drug formulation onto a surface at such a temperature could induce the sol-to-gel transition [54]. As such, a transparent surface adherent film will be formed which prolongs the drug retention on the surface and further leads to an increased therapeutic efficacy.

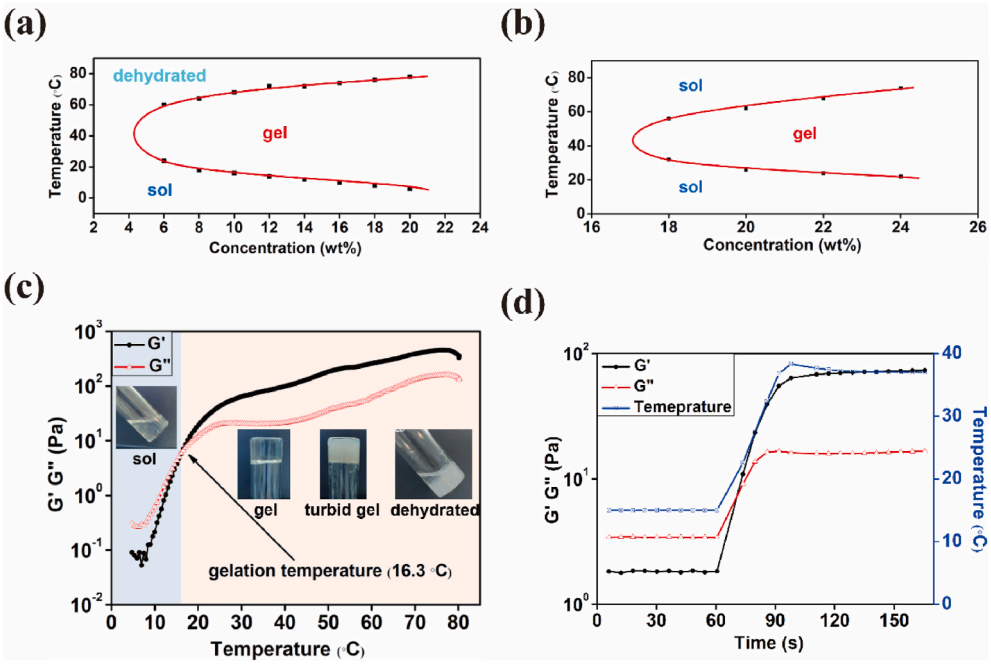

Fig. 4. Phase diagram of (a) 1MPEP and (b) Pluronic F127. Rheological properties of 1MPEP (6 wt%) during a (c) temperature sweep and (d) temperature ramp.

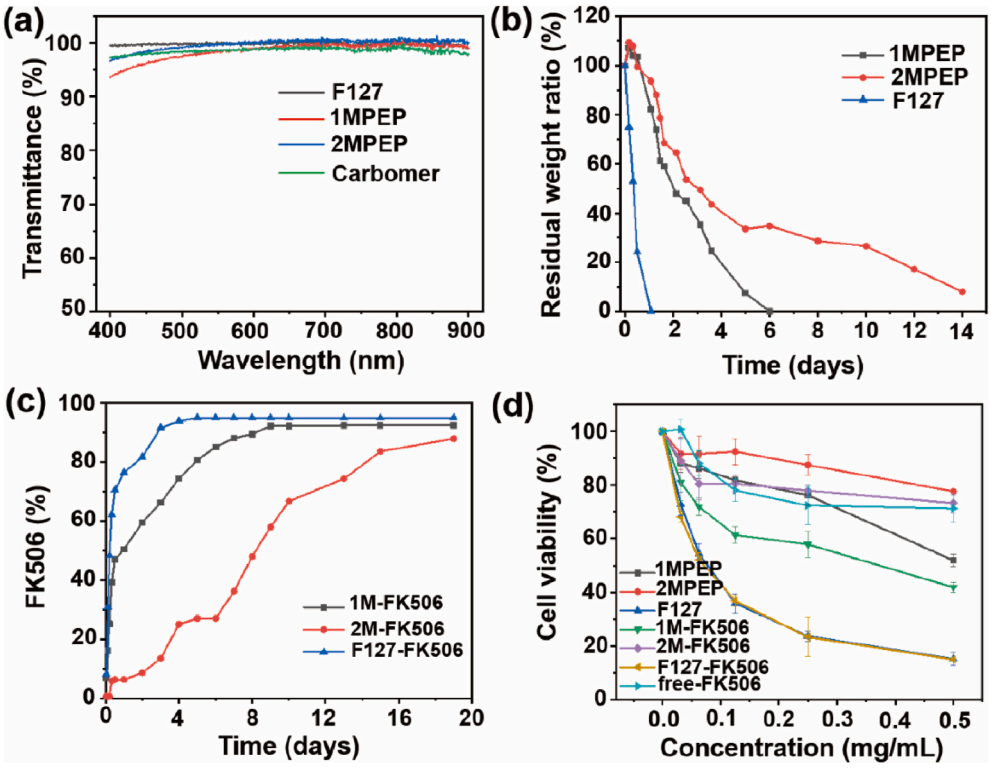

Fig. 5. (a) Determination of the light transmittance of the 1MPEP, 2MPEP, F127, and Commercial carbomer hydrogels. (b) *In vitro* degradation of the 1MPEP, 2MPEP, and F127 hydrogels. (c) *In vitro* drug release behavior of FK506 from the 1MPEP, 2MPEP, and F127 hydrogels. (d) *In vitro* cytotoxicity of the hydrogels toward HCE cells.

3.4. Light transmittance of the blank hydrogel

According to previous studies, hydrogels are considered to be transparent if their light transmittance is greater than 90% over the visible wavelength range of 390–780 nm [37]. Since eye hydrogels require high transparency, we tested the absorbance of 1MPEP, 2MPEP, and F127 after gelling, and calculated the light transmittance according to the formula A = –log T% (Fig. 5a). We found that the light transmittance of the hydrogel was greater than 90% within the visible light wavelength range, indicating that the transparency of 1MPEP, 2MPEP, and F127 is excellent and will not affect vision. In addition, we also calculated the light transmittance of the commercial liquid carbomer

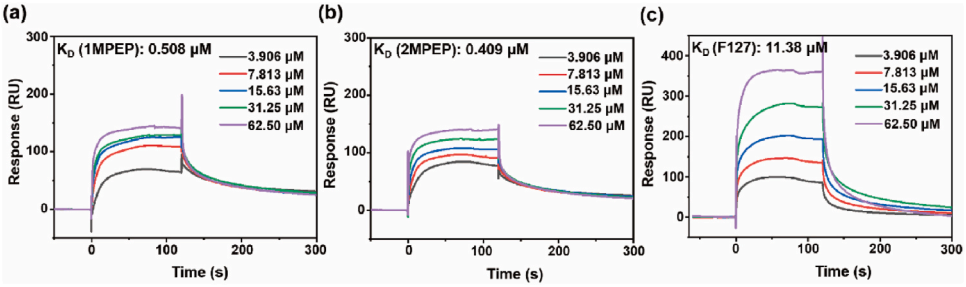

Fig. 6. Surface plasmon resonance was used to evaluate the *in vitro* binding affinity of mucin and (a) 1MPEP, (b) 2MPEP, (c) F127 polymers.

and found that it was not significantly different.

3.5. Degradation of the hydrogel and in vitro release of FK506

Previous studies have shown that it is beneficial to formulate copolymers into the hydrogels for ocular applications, because the hydrogel delivery system used on the ocular surface can not only offer a slow-release rate of encapsulated payloads for stable drug concentration, but also effectively resist the ocular surface clearance mechanism for improving the bioavailability [55,56]. We prepared 1MPEP, 2MPEP, and F127 hydrogels and conducted *in vitro* degradation experiments to compare the degradation rates. As shown in Fig. 5b, the degradation rate of F127 was very fast and almost completely degraded on day 1; however, degradation of the 1MPEP hydrogel was slower and was completely degraded only on day 6, whereas that of the 2MPEP hydrogel was even slower, approaching complete degradation on day 14. The slow degradation of the hydrogel on the ocular surface could reduce the rate at which the drug delivery system turns into an aqueous solution. Such an effect will retard flushing of the drug delivery system from the ocular surface. Besides, the degradation rate of the hydrogel affects the release rate of the drug from the hydrogel. The sustained release of the drug can maintain the drug concentration at a relatively high level on the ocular surface for a longer time. Previous studies compared the pharmacokinetics of topical hydrogels and eye drops, the results indicate that administering a drug in a hydrogel sustains its release and significantly improves its bioavailability. These characteristics also explain the reason for our preference in using a hydrogel formulation as drug delivery system [11,57,58].

Moreover, we prepared 1MPEP, 2MPEP, and F127 hydrogels containing FK506. FK506-loaded polymer micelles were prepared first; the FK506 encapsulation efficiency of 1MPEP and 2MPEP reached 93.4% and 92.8%, respectively, and the FK506 loading capacity was 4.46% and 4.43%, respectively. Subsequently, the blank copolymers were added to reach the correct hydrogel concentration, and the temperature was raised to transform the solution into a gel state. As shown in Fig. S6, in comparison with Commercial FK506, the transparency of the FK506 solution encased in F127, 1MPEP, and 2MPEP polymers was significantly improved, which indicates that the polymer micelles significantly improved the solubility of FK506 in aqueous solution. To explore the FK506 release rate from the hydrogel, an *in vitro* drug release experiment was carried out (Fig. 5c). The results show that FK506 was released fastest from the F127 hydrogel, while it was released slower from the 1MPEP hydrogel, and even more so from the 2MPEP hydrogel, which indicates that the hydrogel containing POSS groups had a higher strength and better slow-release effects.

3.6. In vitro cytotoxicity of the hydrogel

To test the cell compatibility of the hydrogel, we used the MTT assay to evaluate the toxicity of the hydrogel extract towards HCE cells (Fig. 5d). The results showed that irrespective of the presence of FK506, the F127 hydrogel extract displayed the highest cytotoxicity, the 1MPEP extract was much less cytotoxic, and the 2MPEP extract was the least cytotoxic. This may be because the degradation rate of F127 is the fastest, resulting in more material entering the extract whereas the 1MPEP and 2MPEP degradation rates are slower, which accounts for them being less cytotoxic. Since the POSS structure has been proven to have very good biocompatibility [59,60], we used the hydrogel extract method to detect the cytotoxicity of the hydrogel. The degree of degradation of the hydrogel was inconsistent at 24h or 48h. It can be seen from the hydrogel degradation experiment that the degradation rate of 2MPEP is slower than 1MPEP, so the concentration of copolymer leached into the medium is lower, so it appears to be less cytotoxic.

3.7. The interaction between mucin and POSS-polymers

Generally, mucus can interact with additives through electrostatic interactions, van der Waals forces, hydrophobic forces, hydrogen bonds, etc. [61] The mucosal surface of the eyeball is covered by a layer of mucus, whose main component is mucin. Various systems have been used to extend the adhesion of drugs by enhancing their interaction with the mucin on the surface of the eyeball [62,63]. There are reports that POSS-containing polymers can enhance adhesion to mucin since the POSS group facilitates protein anchoring [33,64]. With a view to exploring the mechanism underlying the enhancement of mucosal adhesion by POSS-containing polymers, we used surface plasmon resonance technology (Biacore T200 system) to verify the binding affinity between the polymers and mucin. Binding affinity is generally measured and reported as the equilibrium dissociation constant (KD); the smaller the KD value, the greater the binding affinity of the ligand for its target. As shown in Fig. 6, the binding force between polymer F127 and mucin was relatively weak, with a KD value of approximately 11.380 μM. Interestingly, for the polymers 1MPEP and 2MPEP containing POSS groups, the affinity to mucin was significantly improved, with KD values of 0.508 μM and 0.409 μM, respectively. The results demonstrate that the addition of POSS groups to the polymer chain helps improve its binding affinity to mucin. It is speculated that the strong hydrophobic POSS groups can interact with the exposed hydrophobic domains around mucin [61,65]. Therefore, POSS-containing polymers may be used to improve adhesion of the drug-carrying system to the ocular surface and prolong the drug retention time.

3.8. Hydrogel gelation and retention on the ocular surface and ocular pharmacokinetics studies

In comparison with commonly used eye drops, hydrogels may remain on the ocular surface for a longer period of time, providing more sustained effects [66]. Blinking and tear flushing cause drug loss [67], whereas the adhesive properties of hydrogels contribute to resistance of their removal from the ocular surface. To evaluate the *in situ* thermo-reversible crosslinking of the hydrogels on the ocular surface, slit-lamp and OCT were conducted. The slit-lamp images in Fig. 7a show that no residue remained on the cornea following topical administration of Commercial FK506. In contrast, following topical administration of

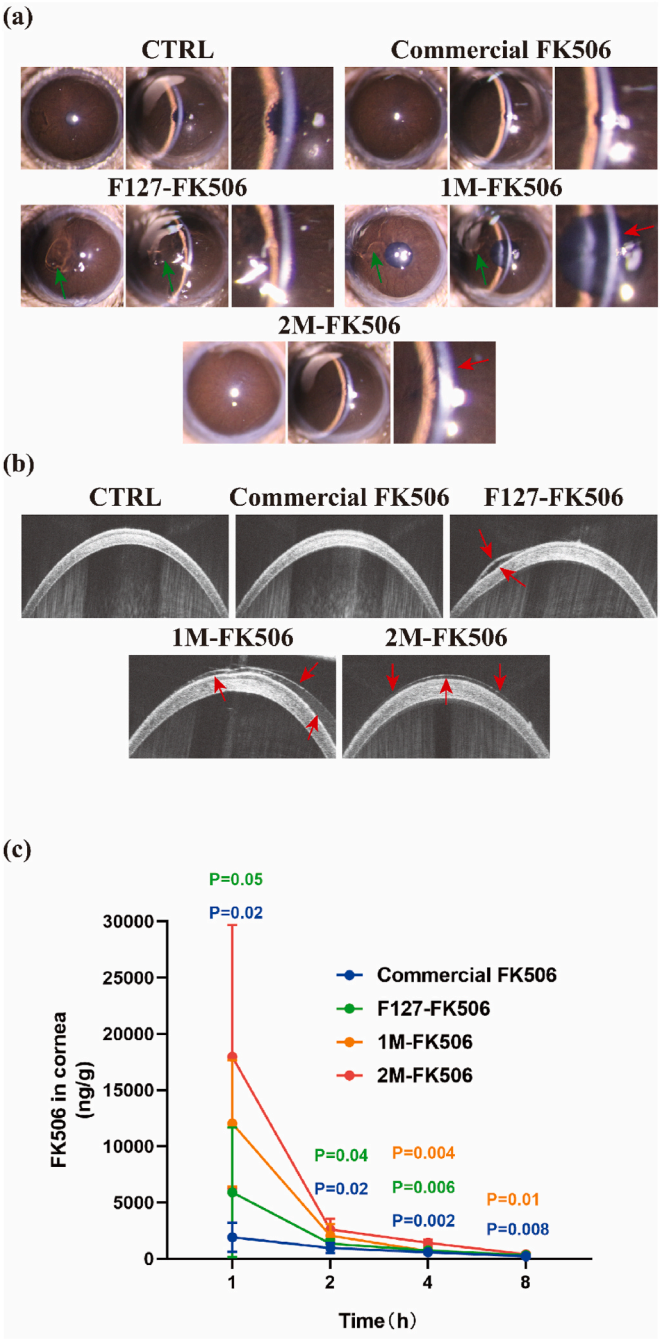

Fig. 7. *In vivo* evaluation of the hydrogels. (a) Slit lamp and (b) OCT images of the hydrogels on the ocular surface after blinking (the red arrow indicates the hydrogel position on the cornea and the green arrow indicates the hydrogel detached from the cornea). (c) Ocular pharmacokinetics studies (n = 4). Data are expressed as the mean ± S.E.M. (For interpretation of the references to colour in this figure legend, the reader is referred to the Web version of this article.)

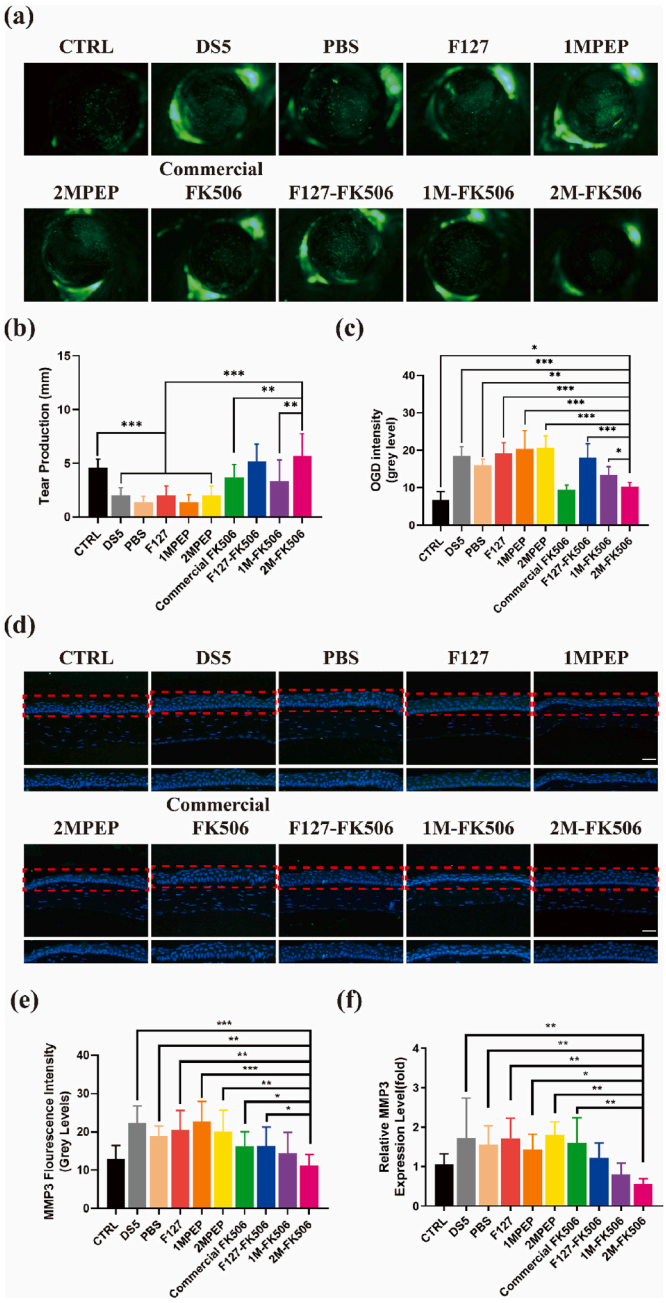

Fig. 8. Images of (a) OGD staining from different groups and (c) OGD intensity statistics (n = 5–7). (b) Tear production was measured using the phenol red thread test (n = 6). (d) Representative images of MMP-3 immunofluorescent staining (the red rectangle shows the area of corneal epithelium MMP-3 immunofluorescence staining). MMP3 staining (e) (n = 5–6) and expression (n = 3–4) (f) quantified. Data are expressed as the mean ± S.E.M. *P < 0.05, **P < 0.01, ***P < 0.001. (For interpretation of the references to colour in this figure legend, the reader is referred to the Web version of this article.)

F127-FK506 (PEG-PPG-FK506), 1M-FK506 (1MPEP-FK506), and 2M-FK506 (2MPEP-FK506), the formulations gelled on the cornea; however, after blinking, the F127-FK506 and 1M-FK506 hydrogels underwent detachment (Fig. 7a, the red arrow indicates the hydrogel position on the cornea and the green arrow indicates the hydrogel detached from the cornea). The 2M-FK506 hydrogel attached well to the cornea and its integrity was not damaged by blinking, suggesting that the 2M-FK506 hydrogel provided stronger adhesion. Subsequently, we attempted to visualize via optical coherence tomography (OCT), its attachment to the cornea surface. The gelation of the F127-FK506 hydrogel resulted in a fragmented coating on the cornea following blinking (red arrow in Fig. 7b, F127-FK506). The 1M-FK506 hydrogel behaved as a nonuniform gel on the cornea after blinking (red arrow in Fig. 7b, 1M-FK506). In contrast, the 2M-FK506 hydrogel formed a smooth gel on the cornea and blinking did not cause loss or damage to the hydrogel (red arrow in Fig. 7b, 2M-FK506), indicating that the 2M-FK506 hydrogel effectively enhanced drug duration on the ocular surface.

In the ocular pharmacokinetics studies, it was observed that 2M-

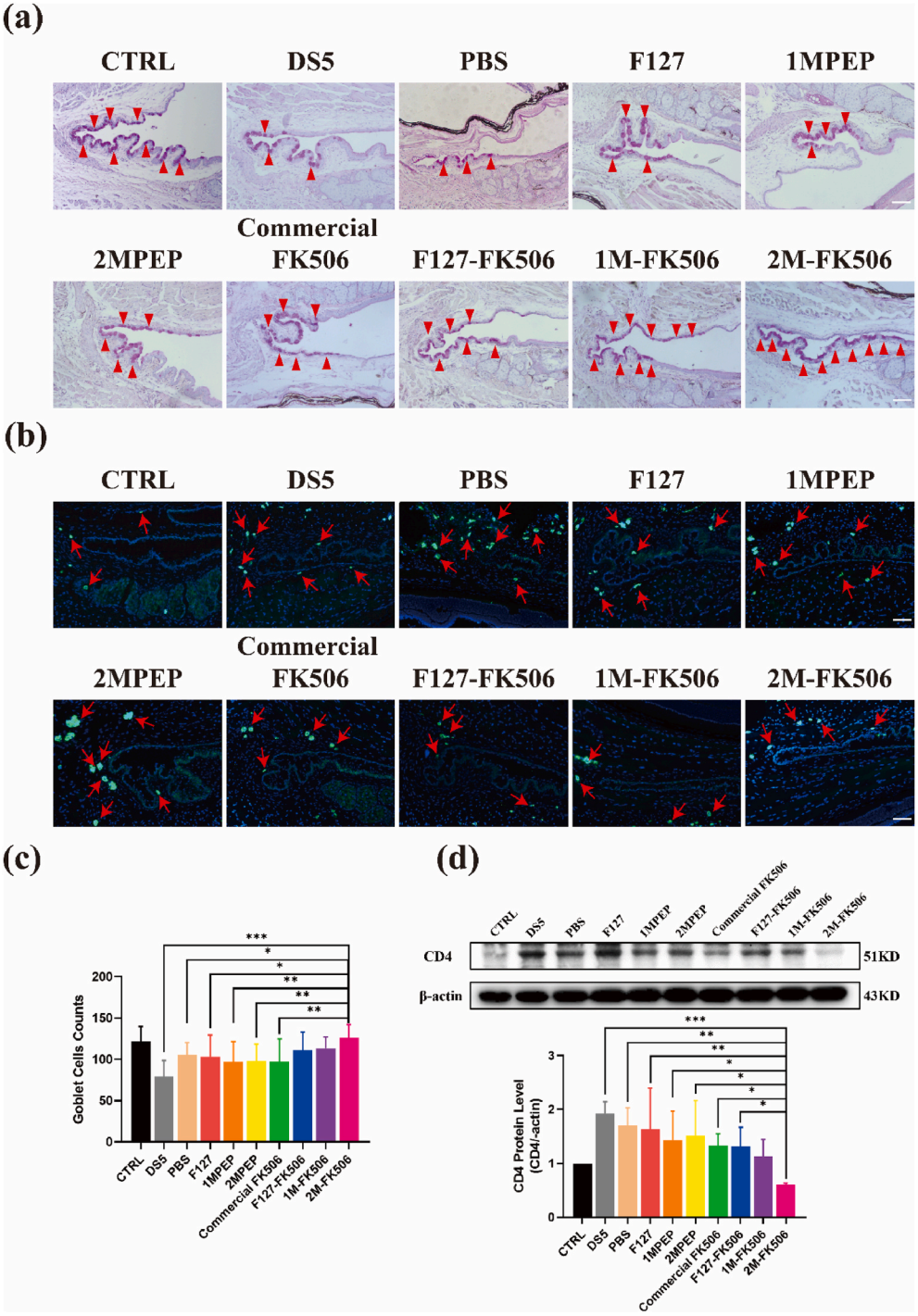

Fig. 9. Histological images of the conjunctiva. (a) PAS staining showing goblet cells in the conjunctiva from each group (the red arrow indicates the goblet cells). (b) CD4 staining showing the number and position of $CD4^+$ T cells infiltrating the conjunctiva from each group (the red arrow indicates $CD4^+$ T cells). Quantitative analysis of the (c) goblet cell counts (n = 8–10) and (d) CD4 protein expression level in the conjunctiva (n = 3). Data are expressed as the mean ± S.E.M. $^*P < 0.05$, $^{**}P < 0.01$, $^{***}P < 0.001$. (For interpretation of the references to colour in this figure legend, the reader is referred to the Web version of this article.)

FK506 provided a significantly increased drug concentrations in rabbit corneas at 1, 2, 4 and 8h after administration compared with F127-FK506 and Commercial FK506 (Fig. 7c). Besides, it could be found that 2M-FK506 provided a significantly increased FK506 concentrations at 1 and 2h after administration compared with 1M-FK506, F127-FK506 and Commercial FK506 in the rabbits' aqueous humor (Fig. S10a and S10b). When compared with F127-FK506, MPEP-FK506 hydrogel effectively resisted the ocular surface clearance by adhering to the ocular surface, which significantly increased the drug concentration of FK506 in the cornea and aqueous humor. Similarly, the thermo-responsive hydrogel system effectively increased the concentration of the FK506 in the cornea and aqueous humor compared to Commercial FK506. Its delivery in the hydrogel system enabled a slow and sustained release of FK506. Therefore, MPEP-FK506 hydrogel with enhanced ocular surface adhesive and thermo-responsive properties was found to increase the efficiency of the ocular surface drug delivery.

3.9. Evaluation of the hydrogels on the dry eye murine model

Different eye drops were used to assess the efficacy of FK506-carrying hydrogels on the murine dry eye model. The cornea was stained using OGD dye and it appeared green in damaged deep-ithelialized regions of the outer layer. As can be seen from Fig. 8a, the OGD staining was severe in the model, DS5, PBS-treated, F127-treated,

1MPEP-treated, and 2MPEP-treated groups; however, the Commercial FK506, F127-FK506, 1M-FK506, and 2M-FK506 groups displayed decreased OGD staining, indicating that these four formulations had good reparative effects on corneal epithelial defects caused by desiccating stress. It is noteworthy that statistical analysis of corneal OGD staining showed that topical application of 2M-FK506 significantly decreased its intensity (Fig. 8c). Owing to stronger adhesion to the cornea, continued slow release of FK506 from this hydrogel protected the corneal epithelium from exposure to a tear deficient environment for a long period of time. Tear production is a very important clinical parameter for the evaluation of the development of dry eye since tears protect the corneal epithelial cells from being lost due to inadequate hydration of the ocular surface [68]. Topical application of 2M-FK506 significantly increased tear production as compared with the other groups, with the exception of F127-FK506, for which the difference was not significant (Fig. 8b). According to these results, 2M-FK506 is an efficient formulation for reversing insufficient tear production due to dry eye.

MMP-3 and MMP-9 expression levels are key indicators of corneal barrier function injuries caused by dry eye; therefore, immunofluorescence staining was employed to determine their levels of MMP-3 and MMP-9 in the corneal epithelium (Fig. 8d, S9). Topical application of Commercial FK506, F127-FK506, 1M-FK506, and 2M-FK506 decreased the expression and staining of MMP-3 in the corneal epithelium. Among these hydrogels, topical application of 2M-FK506 decreased the levels of MMP-3 the most, suggesting improvement of the corneal barrier function under desiccating stress (Fig. 8e, 8f).

Dry eye not only causes damage to the corneal barrier function but also roughens the smooth corneal epithelial surface. According to corneal H&E staining, 2M-FK506 hastened more the recovery of corneal epithelial morphology than that caused by other groups (Fig. S8a). Moreover, goblet cells are simple columnar epithelial cells that secrete mucin to form the tear film, which resists changes in the environment of the ocular surface [69], but inflammation caused by dry eye results in goblet cell loss. The 2M-FK506 hydrogel significantly rescued goblet cell loss under desiccating stress (Fig. 9a, 9c, S8b), indicating that 2M-FK506 suppressed inflammation over a long period of time and played an active role in promoting the recovery of ocular surface injury due to long-term retention of the hydrogel. Dry eye is a chronic inflammatory immune disease characterized by infiltration of $CD4^+$ T cells into the conjunctiva [70]. FK506 (Tacrolimus) binds the immunophilins cyclophilin and FKBP12, which inhibit calcineurin activity and direct the metabolic reprogramming of $CD4^+$ T cells to boost their immunosuppressive effects [71]. The results of the present study indicate that the topical application of 2M-FK506 effectively suppressed the DS-induced infiltration of $CD4^+$ T cells in the conjunctiva (Fig. 9b). Considering that $CD4^+$ T cells play a key role in FK506 treatment of dry eye, the expression of CD4 was further verified. In accordance, 2M-FK506 effectively inhibited the expression of CD4 (Fig. 9d), indicating that 2MPEP allowed greater efficacy of FK506.

3.10. Safety of the hydrogel in mice

Zhu et al. speculated that the induction of a chronic immune response to nanoparticles might injure the layers of retinal vessels, degenerate retinal cells, and induce neovascularization [72]. Depending on the particulate makeup, it may even elicit a systemic inflammatory response. The therapeutic effects of the MPEP-FK506 formulation have previously been explored on the dry eye murine model; however, its safety still requires verification. Therefore, fundus imaging, fluorescence fundus angiography, and OCT examination were performed following topical administration of different formulations for 7 days. Fundus imaging is a common examination technique to observe the morphology of the retina, optic disc, macular area, and retinal blood vessels, as well as whether there is hemorrhage, exudation, hemangioma, retinal degeneration, retinal hiatus, new blood vessels, atrophy spots, pigment

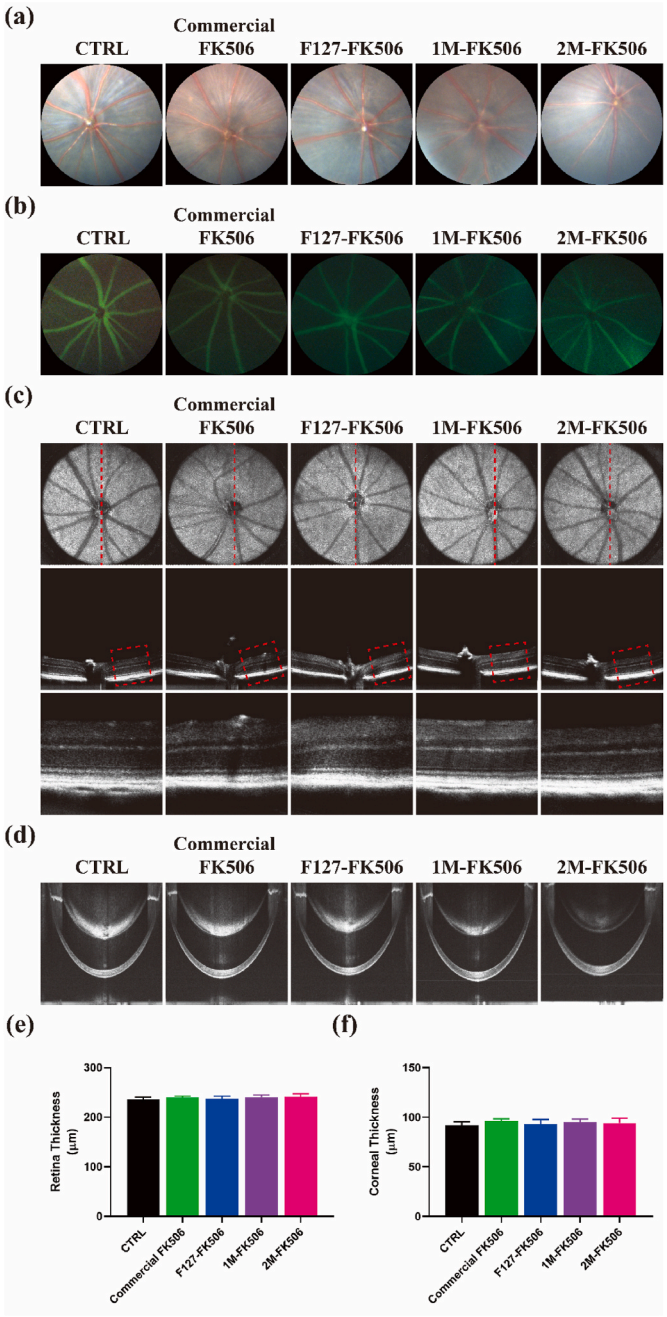

Fig. 10. Safety analysis of hydrogel administration to the ocular surface. (a) Fundus images and (b) fluorescence fundus angiography of eyes from different groups. (c) and (d) OCT images showing the structure and morphology of the retina and cornea (red line indicates a scanning section of the murine retina and the red rectangle shows a partial view of the retina). There is no difference in retinal (e) and corneal (f) thicknesses among the groups (n = 4). Data are expressed as the mean ± S.E.M. (For interpretation of the references to colour in this figure legend, the reader is referred to the Web version of this article.)

disorder, and other changes to the retina [73]. Fundus angiography is mainly used for further observation of tiny structural changes in fundus blood vessels. From the fundus images and fluorescence fundus angiography, no obvious leakage of fundus vessels, vascular enlargement, or abnormal routes were observed after treatment (Fig. 10a, 10b). OCT is a diagnostic technique in ophthalmology that possesses the advantages of being non-invasive, having a high resolution at the cellular level and a fast-imaging speed, and solving the problem of *in vivo* study of the retina and cornea [74]. OCT examination of the retina on day 7 showed that

the structure of each retinal layer was arranged in an orderly fashion with no obvious retinal detachment or degeneration, and no difference was observed in retinal thickness among the groups (Fig. 10c). Besides, the appearance of the cornea remained normal after treatment among the groups (Fig. 10d). Variation in corneal or retinal thickness indicates the presence of pathological lesions. However, the present data shows that hydrogel administration to the ocular surface did not change the thickness of the cornea and retina compared to the control group irrespective of the time of exposure (Fig. 10e, 10f). Therefore, hydrogel administration does not pose any risk to ocular surface health.

4. Conclusion

In summary, we show that an FK506-loaded ocular adhesive thermo-responsive hydrogel using a PEG-PPG (F127) copolymer modified with polyhedral oligomeric silsesquioxane (POSS) groups effectively alleviated dry eye symptomology in mice. MPOSS-PEG-PPG (MPEP) possesses the ability to self-assemble on the ocular surface with suitable micellization and gelation characteristics. Moreover, this hydrogel could load poorly water-soluble FK506 and significantly enhance its ocular surface retention. This hydrogel showed excellent biocompatibility and low toxicity both *in vitro* and *in vivo*. Finally, we found that this POSS thermo-responsive hydrogel inhibited dry eye more efficiently than currently available drugs in a murine model. According to our findings, this POSS thermo-responsive hydrogel shows great application prospects for the development of long-acting ocular treatments for more efficient management of ocular diseases.

CRediT authorship contribution statement

Yi Han: Investigation, Methodology, Formal analysis, Data curation, Writing – original draft. **Lu Jiang:** Methodology, Formal analysis, Data curation, Writing – original draft. **Huihui Shi:** Methodology, Formal analysis, Data curation, Writing – original draft. **Chenfang Xu:** Methodology, Formal analysis, Data curation, Writing – original draft, Visualization. **Minting Liu:** Methodology. **Qingjian Li:** Formal analysis. **Lan Zheng:** Methodology. **Hong Chi:** Methodology. **Mingyue Wang:** Methodology, Project administration, Conceptualization, Supervision, Funding acquisition. **Zuguo Liu:** Supervision, Funding acquisition. **Mingliang You:** Supervision, Funding acquisition. **Xian Jun Loh:** Supervision, Funding acquisition. **Yun-Long Wu:** Project administration, Conceptualization, Supervision, Funding acquisition. **Zibiao Li:** Project administration, Conceptualization, Supervision, Funding acquisition. **Cheng Li:** Project administration, Conceptualization, Supervision, Funding acquisition, Writing – review & editing.

Declaration of competing interest

None of the content of the present paper has been published or submitted to any other journal. All the listed authors reviewed and approved the content prior to submission. None of the authors have any ethical conflicts of interest.

Acknowledgements

Y. Han, L. Jiang, H. Shi and C. Xu contributed equally to this work. This study was supported in part by grants from The National Key R&D Program of China (2020YFA0908100), the National Natural Science Foundation of China (NSFC No. 82070931, 81770891, 81971724, 81773661), the Agency for Science, Technology and Research (A*STAR) under its AME IAF-PP Specialty Chemicals Program (Grant No. A1786a0034), and the Huaxia Translational Medicine Fund for Young Scholars (No. 2017-A-001).

Appendix A. Supplementary data

Supplementary data to this article can be found online at https://doi.org/10.1016/j.bioactmat.2021.07.027.

References

[1] J.P. Craig, et al., TFOS DEWS II report executive summary, Ocul. Surf. 15 (2017) 802–812, https://doi.org/10.1016/j.jtos.2017.08.003.
[2] F. Stapleton, et al., TFOS DEWS II epidemiology report, Ocul. Surf. 15 (2017) 334–365, https://doi.org/10.1016/j.jtos.2017.05.003.
[3] E. Goto, Y. Yagi, Y. Matsumoto, K. Tsubota, Impaired functional visual acuity of dry eye patients, Am. J. Ophthalmol. 133 (2002) 181–186, https://doi.org/10.1016/s0002-9394(01)01365-4.
[4] J.H. Joe, et al., Effect of the solid-dispersion method on the solubility and crystalline property of tacrolimus, Int. J. Pharm. 395 (2010) 161–166, https://doi.org/10.1016/j.ijpharm.2010.05.023.
[5] S. Lin, et al., Overcoming the anatomical and physiological barriers in topical eye surface medication using a peptide-decorated polymeric micelle, ACS Appl. Mater. Interfaces 11 (2019) 39603–39612, https://doi.org/10.1021/acsami.9b13851.
[6] D. Liu, et al., A novel FK506 loaded nanomicelles consisting of amino-terminated poly (ethylene glycol)-block-poly(D,L)-lactic acid and hydroxypropyl methylcellulose for ocular drug delivery, Int. J. Pharm. 562 (2019) 1–10, https://doi.org/10.1016/j.ijpharm.2019.03.022.
[7] C. Civiale, M. Licciardi, G. Cavallaro, G. Giammona, M.G. Mazzone, Polyhydroxyethylaspartamide-based micelles for ocular drug delivery, Int. J. Pharm. 378 (2009) 177–186, https://doi.org/10.1016/j.ijpharm.2009.05.028.
[8] Y. Wu, et al., Research progress of in-situ gelling ophthalmic drug delivery system, Asian J. Pharm. Sci. 14 (2019) 1–15, https://doi.org/10.1016/j.ajps.2018.04.008.
[9] L.-J. Luo, N. Duc Dung, J.-Y. Lai, Long-acting mucoadhesive thermogels for improving topical treatments of dry eye disease, Materials Science & Engineering C-Materials for Biological Applications 115 (2020), 111095, https://doi.org/10.1016/j.msec.2020.111095.
[10] L.-J. Luo, J.-Y. Lai, Epigallocatechin gallate-loaded gelatin-g-poly(N-isopropylacrylamide) as a new ophthalmic pharmaceutical formulation for topical use in the treatment of dry eye syndrome, Sci. Rep. 7 (2017), 9380, https://doi.org/10.1038/s41598-017-09913-8.
[11] C.R. Lynch, et al., Hydrogel biomaterials for application in ocular drug delivery, Frontiers in Bioengineering and Biotechnology 8 (2020), 228, https://doi.org/10.3389/fbioe.2020.00228.
[12] Y.-H. Cheng, Y.-C. Ko, Y.-F. Chang, S.-H. Huang, C.J.-l. Liu, Thermosensitive chitosan-gelatin-based hydrogel containing curcumin-loaded nanoparticles and latanoprost as a dual-drug delivery system for glaucoma treatment, Exp. Eye Res. 179 (2019) 179–187, https://doi.org/10.1016/j.exer.2018.11.017.
[13] W. Zhang, G. Camino, R. Yang, Polymer/polyhedral oligomeric silsesquioxane (POSS) nanocomposites: an overview of fire retardance, Prog. Polym. Sci. 67 (2017) 77–125, https://doi.org/10.1016/j.progpolymsci.2016.09.011.
[14] M.G. Mohamed, S.W. Kuo, Functional polyimide/polyhedral oligomeric silsesquioxane nanocomposites, Polymers 11 (2019), 26, https://doi.org/10.3390/polym11010026.
[15] Z. Li, J. Kong, F. Wang, C. He, Polyhedral oligomeric silsesquioxanes (POSSs): an important building block for organic optoelectronic materials, J. Mater. Chem. C 5 (2017) 5283–5298, https://doi.org/10.1039/C7TC01327B.
[16] M.G. Mohamed, S.W. Kuo, Functional silica and carbon nanocomposites based on polybenzoxazines, Macromol. Chem. Phys. 220 (2019), 1800306, https://doi.org/10.1002/macp.201800306.
[17] M.G. Mohamed, K.-C. Hsu, J.-L. Hong, S.-W. Kuo, Unexpected fluorescence from maleimide-containing polyhedral oligomeric silsesquioxanes: nanoparticle and sequence distribution analyses of polystyrene-based alternating copolymers, Polym. Chem. 7 (2016) 135–145, https://doi.org/10.1039/c5py01537e.
[18] F. Chen, et al., Polyhedral oligomeric silsesquioxane hybrid polymers: well-defined architectural design and potential functional applications, Macromol. Rapid Commun. 40 (2019), 1900101, https://doi.org/10.1002/marc.201900101.
[19] S. Kuo, F. Chang, POSS related polymer nanocomposites, Prog. Polym. Sci. 36 (2011) 1649–1696, https://doi.org/10.1016/j.progpolymsci.2011.05.002.
[20] H. Zhao, et al., Fabrication and properties of waterborne thermoplastic polyurethane nanocomposite enhanced by the POSS with low dielectric constants, Polymer 209 (2020), 122992, https://doi.org/10.1016/j.polymer.2020.122992.
[21] M.G. Mohamed, N.-Y. Liu, A.F.M. El-Mahdy, S.-W. Kuo, Ultrastable luminescent hybrid microporous polymers based on polyhedral oligomeric silsesquioxane for CO2 uptake and metal ion sensing, Microporous Mesoporous Mater. 311 (2021), 110695, https://doi.org/10.1016/j.micromeso.2020.110695.
[22] S.J. Buwalda, et al., Hydrogels in a historical perspective: from simple networks to smart materials, J. Contr. Release 190 (2014) 254–273, https://doi.org/10.1016/j.jconrel.2014.03.052.
[23] A. Vedadghavami, et al., Manufacturing of hydrogel biomaterials with controlled mechanical properties for tissue engineering applications, Acta Biomater. 62 (2017) 42–63, https://doi.org/10.1016/j.actbio.2017.07.028.
[24] N. Eslahi, M. Abdorahim, A. Simchi, Smart polymeric hydrogels for cartilage tissue engineering: a review on the Chemistry and biological functions, Biomacromolecules 17 (2016) 3441–3463, https://doi.org/10.1021/acs.biomac.6b01235.
[25] J. Li, D.J. Mooney, Designing hydrogels for controlled drug delivery, Nature reviews. Materials 1 (2016), 16071, https://doi.org/10.1038/natrevmats.2016.71.

[26] E.A. Kamoun, E.-R.S. Kenawy, X. Chen, A review on polymeric hydrogel membranes for wound dressing applications: PVA-based hydrogel dressings, J. Adv. Res. 8 (2017) 217–233, https://doi.org/10.1016/j.jare.2017.01.005.
[27] Y. Chen, G. Zeng, W. Liu, Robust and stimuli-responsive POSS hybrid PDMAEMA hydrogels for controlled drug release, J. Biomed. Mater. Res. 104 (2016) 2345–2355, https://doi.org/10.1002/jbm.a.35771.
[28] D. Prządka, E. Andrzejewska, A. Marcinkowska, Multimethacryloxy-POSS as a crosslinker for hydrogel materials, Eur. Polym. J. 72 (2015) 34–49, https://doi.org/10.1016/j.eurpolymj.2015.09.007.
[29] Y. Chen, et al., Synthesis and characterization of polyhedral oligomeric silsesquioxane hybrid co-crosslinked poly(N-isopropylacrylamide-co-dimethylaminoethyl methacrylate) hydrogels, J. Polym. Sci. B Polym. Phys. 51 (2013) 1494–1504, https://doi.org/10.1002/polb.23360.
[30] X. Zhang, et al., Enhanced mechanical properties and self-healing behavior of PNIPAM nanocomposite hydrogel by using POSS as a physical crosslinker, J. Appl. Polym. Sci. 137 (2020), 48486, https://doi.org/10.1002/app.48486.
[31] Z. Qin, et al., Injectable shear-thinning hydrogels with enhanced strength and temperature stability based on polyhedral oligomeric silsesquioxane end-group aggregation, Polym. Chem. 8 (2017) 1607–1610, https://doi.org/10.1039/C6PY02180H.
[32] J. Wu, Q. Ge, P.T. Mather, PEG−POSS multiblock polyurethanes: synthesis, characterization, and hydrogel formation, Macromolecules 43 (2010) 7637–7649, https://doi.org/10.1021/ma101336c.
[33] M. Chen, Y. Zhang, W. Zhang, J. Li, Polyhedral oligomeric silsesquioxane-incorporated gelatin hydrogel promotes angiogenesis during vascularized bone regeneration, ACS Appl. Mater. Interfaces 12 (2020) 22410–22425, https://doi.org/10.1021/acsami.0c00714.
[34] B.Q. Chan, et al., Poly(carbonate urethane)-based thermogels with enhanced drug release efficacy for chemotherapeutic applications, Polymers 10 (2018), 89, https://doi.org/10.3390/polym10010089.
[35] Y. Yu, et al., A hybrid genipin-crosslinked dual-sensitive hydrogel/nanostructured lipid carrier ocular drug delivery platform, Asian J. Pharm. Sci. 14 (2019) 423–434, https://doi.org/10.1016/j.ajps.2018.08.002.
[36] W. Mäntele, E. Deniz, UV–VIS absorption spectroscopy: lambert-Beer reloaded, Spectrochim. Acta Mol. Biomol. Spectrosc. 173 (2017) 965–968, https://doi.org/10.1016/j.saa.2016.09.037.
[37] X. Li, Z. Zhang, H. Chen, Development and evaluation of fast forming nano-composite hydrogel for ocular delivery of diclofenac, Int. J. Pharm. 448 (2013) 96–100, https://doi.org/10.1016/j.ijpharm.2013.03.024.
[38] S. Narayanan, R.M. Corrales, W. Farley, A.M. McDermott, S.C. Pflugfelder, Interleukin-1 receptor-1-deficient mice show attenuated production of ocular surface inflammatory cytokines in experimental dry eye, Cornea 27 (2008) 811–817, https://doi.org/10.1097/ICO.0b013e31816bf46c.
[39] C.S. de Paiva, C.E. Schwartz, P. Gjoerstrup, S.C. Pflugfelder, Resolvin E1 (RX-10001) reduces corneal epithelial barrier disruption and protects against goblet cell loss in a murine model of dry eye, Cornea 31 (2012) 1299–1303, https://doi.org/10.1097/ICO.0b013e31823f789e.
[40] J.T. Henriksson, et al., Morphologic alterations of the palpebral conjunctival epithelium in a dry eye model, Cornea 32 (2013) 483–490, https://doi.org/10.1097/ICO.0b013e318265682c.
[41] Y. Han, et al., Studies on bacterial cellulose/poly(vinyl alcohol) hydrogel composites as tissue-engineered corneal stroma, Biomed. Mater. 15 (2020), 035022, https://doi.org/10.1088/1748-605X/ab56ca.
[42] H. Shi, et al., Self-healable, fast responsive poly(ω-pentadecalactone) thermogelling system for effective liver cancer therapy, Frontiers in Chemistry 7 (2019), 683, https://doi.org/10.3389/fchem.2019.00683.
[43] G. Gultekin, et al., Fatty acid-based polyurethane films for wound dressing applications, J. Mater. Sci. Mater. Med. 20 (2009) 421–431, https://doi.org/10.1007/s10856-008-3572-5.
[44] J.H. Moon, J. Seo, Y. Xu, S. Yang, Direct fabrication of 3D silica-like microstructures from epoxy-functionalized polyhedral oligomeric silsesquioxane (POSS), Journal of Materials Chemistry - J MATER CHEM 19 (2009) 4687–4691, https://doi.org/10.1039/b901226e.
[45] B. Sadhasivam, S. Muthusamy, Thermal and dielectric properties of newly developed L-tryptophan-based optically active polyimide and its POSS nanocomposites, Des. Monomers Polym. 19 (2016) 236–247, https://doi.org/10.1080/15685551.2015.1136530.
[46] H. Celik, M. Kodal, B. Karaagac, G. Ozkoc, Effects of octamaleamic acid-POSS used as the adhesion enhancer on the properties of silicone rubber/silica nanocomposites, Compos. B Eng. 98 (2016) 370–381, https://doi.org/10.1016/j.compositesb.2016.05.024.
[47] K. Tsobkallo, et al., Effect of the morphology of reactor powders on the structure and mechanical behavior of drawn ultra-high molecular weight polyethylenes, Polymer 44 (2003) 1613–1618, https://doi.org/10.1016/S0032-3861(02)00909-6.
[48] Z. Sezgin, N. Yüksel, T. Baykara, Preparation and characterization of polymeric micelles for solubilization of poorly soluble anticancer drugs, Eur. J. Pharm. Biopharm. 64 (2006) 261–268, https://doi.org/10.1016/j.ejpb.2006.06.003.
[49] Z. Li, Z. Zhang, K.L. Liu, X. Ni, J. Li, Biodegradable hyperbranched amphiphilic polyurethane multiblock copolymers consisting of poly(propylene glycol), poly (ethylene glycol), and polycaprolactone as in situ thermogels, Biomacromolecules 13 (2012) 3977–3989, https://doi.org/10.1021/bm3012506.
[50] H. Hussain, et al., Micelle formation and gelation of (PEG−P(MA-POSS)) amphiphilic block copolymers via associative hydrophobic effects, Langmuir 26 (2010) 11763–11773, https://doi.org/10.1021/la101686q.
[51] B.H. Tan, H. Hussain, C.B. He, Tailoring micelle formation and gelation in (PEG−P(MA-POSS)) amphiphilic hybrid block copolymers, Macromolecules 44 (2011) 622–631, https://doi.org/10.1021/ma102510u.
[52] S.S. Liow, et al., Thermogels: in situ gelling biomaterial, ACS Biomater. Sci. Eng. 2 (2016) 295–316, https://doi.org/10.1021/acsbiomaterials.5b00515.
[53] P. Groch, K. Czaja, U. Szeluga, S. Rabiej, M. Baczek, The effect of macromolecular architecture of ethylene copolymers with multi-alkenylsilsesquioxane on morphological, rheological and dynamic mechanical behavior, Polymer 212 (2021), 123172, https://doi.org/10.1016/j.polymer.2020.123172.
[54] N. Efron, G. Young, N.A. Brennan, Ocular surface-temperature, Curr. Eye Res. 8 (1989) 901–906.
[55] S. Kirchhof, A.M. Goepferich, F.P. Brandl, Hydrogels in ophthalmic applications, Eur. J. Pharm. Biopharm. 95 (2015) 227–238, https://doi.org/10.1016/j.ejpb.2015.05.016.
[56] S. Deepthi, J. Jose, Novel hydrogel-based ocular drug delivery system for the treatment of conjunctivitis, Int. Ophthalmol. 39 (2019) 1355–1366, https://doi.org/10.1007/s10792-018-0955-6.
[57] Y.A. Gao, Y. Sun, F.Z. Ren, S. Gao, PLGA-PEG-PLGA hydrogel for ocular drug delivery of dexamethasone acetate, Drug Dev. Ind. Pharm. 36 (2010) 1131–1138, https://doi.org/10.3109/03639041003680826.
[58] M. Jamard, T. Hoare, H. Sheardown, Nanogels of methylcellulose hydrophobized with N-tert-butylacrylamide for ocular drug delivery, Drug Delivery and Translational Research 6 (2016) 648–659, https://doi.org/10.1007/s13346-016-0337-4.
[59] C.H. Shen, et al., Ocular biocompatibility evaluation of POSS nanomaterials for biomedical material applications, RSC Adv. 5 (2015) 53782–53788, https://doi.org/10.1039/c5ra08668j.
[60] H. Ghanbari, B.G. Cousins, A.M. Seifalian, A nanocage for nanomedicine: polyhedral oligomeric silsesquioxane (POSS), Macromol. Rapid Commun. 32 (2011) 1032–1046, https://doi.org/10.1002/marc.201100126.
[61] J. Woodley, Bioadhesion - New possibilities for drug administration? Clin. Pharmacokinet. 40 (2001) 77–84, https://doi.org/10.2165/00003088-200140020-00001.
[62] Y.S. Chhonker, et al., Amphotericin-B entrapped lecithin/chitosan nanoparticles for prolonged ocular application, Int. J. Biol. Macromol. 72 (2015) 1451–1458, https://doi.org/10.1016/j.ijbiomac.2014.10.014.
[63] J. Li, et al., Positively charged micelles based on a triblock copolymer demonstrate enhanced corneal penetration, Int. J. Nanomed. 10 (2015) 6027–6037, https://doi.org/10.2147/IJN.S90347.
[64] S. Tamburaci, F. Tihminlioglu, Chitosan-hybrid poss nanocomposites for bone regeneration: the effect of poss nanocage on surface, morphology, structure and in vitro bioactivity, Int. J. Biol. Macromol. 142 (2020) 643–657, https://doi.org/10.1016/j.ijbiomac.2019.10.006.
[65] M. Liu, J. Zhang, W. Shan, Y. Huang, Developments of mucus penetrating nanoparticles, Asian J. Pharm. Sci. 10 (2015) 275–282, https://doi.org/10.1016/j.ajps.2014.12.007.
[66] Y.C. Kim, et al., Gelling hypotonic polymer solution for extended topical drug delivery to the eye, Nature Biomedical Engineering 4 (2020) 1053–1062, https://doi.org/10.1038/s41551-020-00606-8.
[67] C.G. Park, et al., Mucoadhesive microparticles with a nanostructured surface for enhanced bioavailability of glaucoma drug, J. Contr. Release 220 (2015) 180–188, https://doi.org/10.1016/j.jconrel.2015.10.027.
[68] F. Yu, M. Zheng, A.Y. Zhang, Z. Han, A cerium oxide loaded glycol chitosan nano-system for the treatment of dry eye disease, J. Contr. Release 315 (2019) 40–54, https://doi.org/10.1016/j.jconrel.2019.10.039.
[69] X. Zhang, et al., Topical application of mizoribine suppresses CD4(+) T-cell-mediated pathogenesis in murine dry eye, Invest. Ophthalmol. Vis. Sci. 58 (2017) 6056–6064, https://doi.org/10.1167/iovs.17-22852.
[70] J.Y. Niederkorn, et al., Desiccating stress induces T cell-mediated Sjogren's syndrome-like lacrimal keratoconjunctivitis, J. Immunol. 176 (2006) 3950–3957, https://doi.org/10.4049/jimmunol.176.7.3950.
[71] A.A. Fernandez-Ramos, V. Poindessous, C. Marchetti-Laurent, N. Pallet, M.-A. Loriot, The effect of immunosuppressive molecules on T-cell metabolic reprogramming, Biochimie 127 (2016) 23–36, https://doi.org/10.1016/j.biochi.2016.04.016.
[72] S. Zhu, et al., Safety assessment of nanomaterials to eyes: an important but neglected issue, Advanced Science 6 (2019), 1802289, https://doi.org/10.1002/advs.201802289.
[73] J. Staal, M.D. Abramoff, M. Niemeijer, M.A. Viergever, B. van Ginneken, Ridge-based vessel segmentation in color images of the retina, IEEE Trans. Med. Imag. 23 (2004) 501–509, https://doi.org/10.1109/tmi.2004.825627.
[74] R.F. Spaide, H. Koizumi, M.C. Pozonni, Enhanced depth imaging spectral-domain optical coherence tomography, Am. J. Ophthalmol. 146 (2008) 496–500, https://doi.org/10.1016/j.ajo.2008.05.032.